NIST Special Publication 260
NIST SP 260-255

Certification of Standard Reference Material® 1989

Monodisperse Irregularly Shaped Epoxy-Based Particles (Nominal 100 µm, 150 µm, 220 µm)

Srivalli N. Telikepalli
Dean C. Ripple
Michael Carrier
Kristen L. Steffens
David Newton
Christopher Montgomery
Nicholas W. M. Ritchie
Anthony J. Asmar
Michael Halter

This publication is available free of charge from:
https://doi.org/10.6028/NIST.SP.260-255

NIST NATIONAL INSTITUTE OF STANDARDS AND TECHNOLOGY
U.S. DEPARTMENT OF COMMERCE

NIST Special Publication 260
NIST SP 260-255

Certification of Standard Reference Material® 1989

Monodisperse Irregularly Shaped Epoxy-Based Particles (Nominal 100 µm, 150 µm, 220 µm)

Srivalli N. Telikepalli
Dean C. Ripple
Michael Carrier
Kristen L. Steffens
Christopher Montgomery
Biomolecular Measurement Division
Materials Measurement Laboratory

David Newton
Statistical Engineering Division
Information Technology Laboratory

Nicholas W. M. Ritchie
Materials Measurement Science Division
Materials Measurement Laboratory

Anthony J. Asmar
Michael Halter
Biosystems and Biomaterials Division
Materials Measurement Laboratory

**Retired NIST employee. All work for this publication was done while at NIST.*

This publication is available free of charge from:
https://doi.org/10.6028/NIST.SP.260-255

May 2025

U.S. Department of Commerce
Howard Lutnick, Secretary

National Institute of Standards and Technology
Craig Burkhardt, Acting Under Secretary of Commerce for Standards and Technology and Acting NIST Director

NIST SP 260-255
May 2025

Certain equipment, instruments, software, or materials, commercial or non-commercial, are identified in this paper in order to specify the experimental procedure adequately. Such identification does not imply recommendation or endorsement of any product or service by NIST, nor does it imply that the materials or equipment identified are necessarily the best available for the purpose.

NIST Technical Series Policies
Copyright, Use, and Licensing Statements
NIST Technical Series Publication Identifier Syntax

Publication History
Approved by the NIST Editorial Review Board on 2025-03-14

How to Cite this NIST Technical Series Publication
Telikepalli SN, Ripple DC, Carrier M, Steffens KL, Newton D, Montgomery C, Ritchie NWM, Asmar AJ, Halter M (2025) Certification of Standard Reference Material® 1989: Monodisperse Irregularly Shaped Epoxy-Based Particles (Nominal 100 µm, 150 µm, 220 µm). (National Institute of Standards and Technology, Gaithersburg, MD), NIST Special Publication 260 (SP) NIST SP 260-255. https://doi.org/10.6028/NIST.SP.260-255

NIST Author ORCID iDs
Srivalli N. Telikepalli: 0000-0003-4687-6123
Dean C. Ripple: 0000-0002-6413-1339
Michael Carrier: 0000-0002-9962-2496
Kristen L. Steffens: 0000-0002-3883-2131
Christopher Montgomery: 0000-0003-0265-6524
David Newton: 0000-0003-3382-8034
Nicholas W. M. Ritchie: 0000-0001-5734-5729
Anthony J Asmar: 0000-0002-4843-0785
Michael Halter: 0000-0002-1628-324X

Technical Information Contact Information for this SRM
Please address technical questions about this SRM to srms@nist.gov where they will be assigned to the appropriate Technical Project Leader responsible for support of this material. For sales and customer service inquiries, please contact srms@nist.gov.

Abstract

Standard Reference Material (SRM) 1989 is a NIST particle standard produced using photolithographic methods, which delivers a certified value for the particle size of an irregularly shaped particle. This SRM was developed to allow more uniform monitoring of visible protein-like particles that may be found in biotherapeutics. The material is intended to be used as a particle size standard for qualifying and training visual inspection analysts on the visual inspection processes. One unit of SRM 1989 contains three (3) vials of irregularly shaped particles that are each monodisperse in terms of size and morphology. The 3 vials consist of particles that have Area-Based Diameters of nominally 100 µm, 150 µm, and 220 µm and Maximum Feret Diameters of nominally 1.5 × the area-based diameter. These sizes were measured using both experimental optical and electronic microscopy methods. Apparent size was obtained predominantly from the optical systems, while the actual size was obtained by correcting for diffraction effects arising from the experimental methods. This publication provides information on the production, measurement, and statistical determination of the uncertainties involved in the certification of SRM 1989.

Keywords

Aggregate, Protein Particles, Protein Particle Surrogate, Photolithographic Particles, Photoresist, Reference Material, Standard, Standard Reference Material (SRM), Visible Particle, Visual Inspection

Abbreviations

A_b	Area of the border
A_f	Area of the filled image
ABD_{act}	Actual Area Based Diameter
ABD_{opt}	Apparent Optical Area Based Diameter
SEM	Scanning Electron Microscope
ABD_{SEM}	Original Area Based Diameter from Scanning Electron Microscopy (SEM) image analysis
MFD	Maximum Feret Diameter
MFD_{SEM}	Original Maximum Feret Diameter from Scanning Electron Microscopy (SEM) image analysis
C_{ABD}	ABD Correction Factor; scaling factors obtained from the measured ratios *R* of the optically determined chord length to that determined on the SEM image. The correction factor for ABD is the geometric average of the chord ratios in two orthogonal directions.
C_F	Maximum Feret Diameter correction factor: scaling factors obtained from the measured ratio *R* of the optically determined chord length to that determined on the SEM image. The correction factor for the maximum Feret is the ratio for the chord aligned with the maximum Feret axis.
FI	Flow Imaging; Microflow Imaging (MFI) and Flow Cam are examples of an FI system.
DIUF	Deionized Ultra-filtered water; also known as Type 1 ultrapure water

Definitions

Area-Based Diameter (ABD) – The diameter of a circle whose area contains the same number of pixels as a particle in a binary image; also known as Equivalent Circular Diameter (ECD). Before calculating this diameter, the internal holes in the particle are filled.

Apparent Diameter – The diameter obtained from the analysis of an optical image. These can be described in terms of Area-Based Diameter or Maximum Feret Diameter.

Actual Diameter – The true diameter of a particle. These can be described in terms of Area-Based Diameter or Maximum Feret Diameter.

Maximum Feret Diameter (MFD) –The maximum distance between two parallel planes touching a particle border but not intruding into the particle interior.

Equivalent Circular Diameter (ECD) – The diameter of a circle whose area contains the same number of pixels as a particle in a binary image; equivalent to Area-Based Diameter (ABD). Before calculating this diameter, the internal holes in the particle are filled.

Type A Uncertainty – Uncertainty that is calculated from a series of observations using statistical analysis.

Type B Uncertainty -Uncertainty in the measurement that is evaluated based on available information, through scientific judgment, rather than through direct measurements.

Experimental Standard Deviation of the Mean (ESDM) – Measure of how much the sample mean (or average) of a set of measurements is expected to vary from the true population mean. It is calculated by dividing the standard deviation of the sample by the square root of the number of measurements, reflecting the precision of the mean estimate.

Optical Resolution – The ability of an optical system to distinguish between two closely spaced objects or points. It is measured as the smallest distance between two points that can still be distinctly identified as separate.

Table of Contents

List of Tables

List of Figures

1. Introduction

Visual inspection of biotherapeutics is an important step for drug manufacturers to obtain regulatory approval and lot release of drug products. USP Chapter 1 requires that every parenteral unit be visually inspected (100 % visual inspection) to ensure that the batch is "essentially free" of particles as well as other defects. It is done to ensure that the product does not contain any unintended particles (or other defects) since their presence can impact the safety and quality of a product. For those products containing proteinaceous particles, manufacturers need to minimize them to the extent possible and show that those particles do not pose any safety concerns. Particles such as these have been implicated in immunogenicity concerns when they are present in some biological products (1-5).

Visual inspection is primarily done by trained, qualified human analysts. For manual inspection, inspectors look at each vial under defined background and lighting conditions to determine if the vial "passes" or "fails" the pre-established "essentially free" criteria regarding particles (6). This type of measurement is very subjective and determined by many factors (6, 7). Standards can be useful to train and qualify analysts for visual inspection. However, an appropriate visible particle standard that can be useful in this regard has not been commercially available.

NIST has received numerous inquiries from many organizations regarding the production of a visible protein-like particle standard. These requests have come from scientists in the biopharmaceutical industry, instrument vendors, and from the U.S. Food and Drug Administration. In the absence of suitable standards, the industry has relied on spherical polystyrene beads that do not look or behave like proteinaceous particles or proprietary standards that are inaccessible to other companies. This makes detecting, monitoring, and trending the stability of proteinaceous visible particles in biotherapeutics challenging. Having a visible, protein-like particle standard is important from a regulatory perspective as it can help better define what is meant by "visible" as this is often a matter of discussion in the field. A physical standard can help better establish what is considered a "visible particle" for a particular product.

An interlaboratory study conducted by our group illustrated that one of the standards under development, the SU-8 photoresist photolithographic particles, can be a suitable tool to aid in visual inspection practices (8). The study highlighted that these photolithographic SU-8 particles can be used to 1) serve as a particle size standard for irregularly shaped particles; 2) train and qualify analysts who perform routine visual inspection of biotherapeutics and allow them to better define visibility of particles; 3) and establish detection thresholds or sensitivity limits for visual inspection methodologies.

Based on feedback from participants in the interlaboratory study, our group decided to develop an SRM composed of SU-8 photolithographic particles of nominally 100 µm Area-Based Diameter (ABD or also referred to in this document as equivalent circular diameter, ECD), 150

µm ABD, and 220 µm ABD in size. These three sizes were chosen based on participant feedback and through considerations of what particle sizes are feasible with our photolithographic method. These particles were fabricated from a commercially available epoxy-based photoresist commonly referred to as SU-8 and produced using photolithographic methods. The particles were prepared in aqueous solution and filled in-house into a total of 630 vials (210 vials per size). This SRM is labeled as SRM 1989 and each unit is comprised of 3 vials: 1 vial of particle suspension for each size. Each vial contains 20 mL of the particle suspension. This SRM is a particle size standard so the certified values will be provided for the particle size. Number concentration will be provided as a value of potential interest to users.

In this document, we will briefly describe the production of the SRM, vial filling, and certification of the size. This work was done at NIST, with particle production conducted at the NIST Center for Nanoscale Science and Technology (NanoFab) facility.

In this report, we used 2 optical microscopes to collect the optical or apparent size of the particles. Additional measurements of the same particles on both an optical and scanning electron microscope (SEM) were used to evaluate the difference between the apparent size and the actual physical size of the particles. This difference is then a correction that can be applied to the experimentally determined apparent size to obtain the actual size. Both the apparent and actual size values are reported as the certified measurements along with uncertainty values. We also measured particle number concentration, where we employed a microscopic method to count the particles.

We envision that these standards will be implemented as size standards for training visual inspectors in industry and perhaps will extend to being used for developing and qualifying automated visual inspection methodologies.

2. SRM 1989 Specifications

The target specifications for this SRM are the following:

- Certified particle sizes expressed in Area Based Diameter (ABD, apparent and actual size), and Maximum Feret Diameter (MFD, apparent and actual size) along with associated uncertainty for each value, where apparent size is the optically measured size
- Particle size traceable to the International System of Units (SI). The NIST-calibrated stage micrometer provides a length reference that is traceable to the SI for length. The size of the particles, defined as ABD (or ECD) is traced back to this measurement
- Particle number concentration of nominally 100 mL^{-1} per vial, at each of the 3 size ranges
- 1 SRM 1989 unit composed of 3, 30 mL vials, with each vial containing 20 mL aqueous suspension of particles of nominally 100 µm ABD, 150 µm ABD, and 220 µm ABD
- Suspensions free of non-SU-8 photolithographic particles or other contaminations to the extent possible
- Solution comprising 0.01 % (w/v) Triton X-100 and 0.02 % (w/v) of sodium azide
- Shelf life of five years for maintaining the size stability of the particles

3. Production of SRM 1989

SRM 1989 is composed of photolithographic particles of 3 sizes, nominally 100 µm ABD, 150 µm ABD, and 220 µm ABD, as shown below in Figure 1. The particles are made from epoxy-based SU-8 photoresist, textured with numerous through-holes, and have a slight flexibility or bowing when in an aqueous solution. These internal through-holes make the relatively flat surface less reflective. The SU-8 photoresist was chosen as it is chemically resistant and stable.

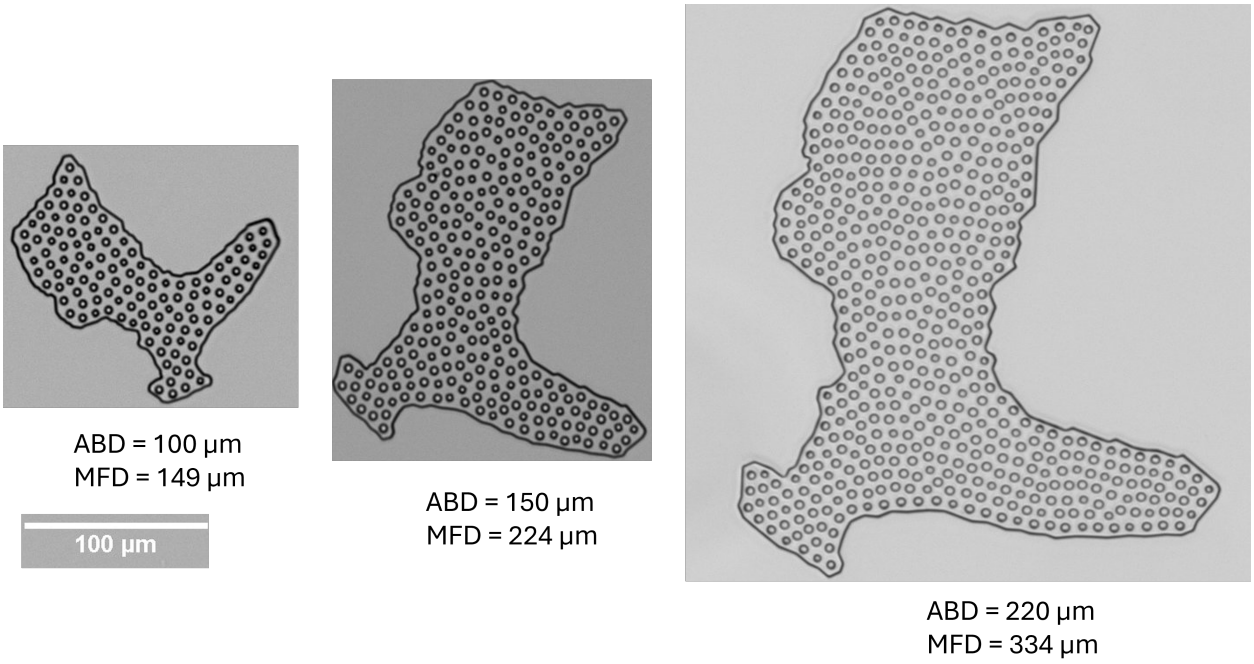

Figure 1. Relative sizes of the three particle types, as obtained by light microscopy

The particles in SRM 1989 have the following properties:

- Uniform particle size and shape
- Square side walls to simplify sizing
- Clean interior features, to allow center-to-center distance finding between holes
- Thin enough to flex slightly, but thick enough to not curl
- Sufficiently free of internal stress to lie flat, at least within the depth of field at 10x magnification
- Smooth surfaces, to ensure long-term stability
- Size in the visible range (> 100 µm)

The general procedure to produce SRM 1989 that satisfies the criteria above is shown in Figure 2. These steps are composed of fabricating the particles in multiple lots, releasing them into solution, inspecting and prescreening the particles for quality, purifying, combining acceptable lots, and filling vials. Particle fabrication was performed at the NIST NanoFab facility.

Purification, vial filling, and characterization were all done in-house at NIST. Optimal experimental conditions that satisfy the above criteria are described below.

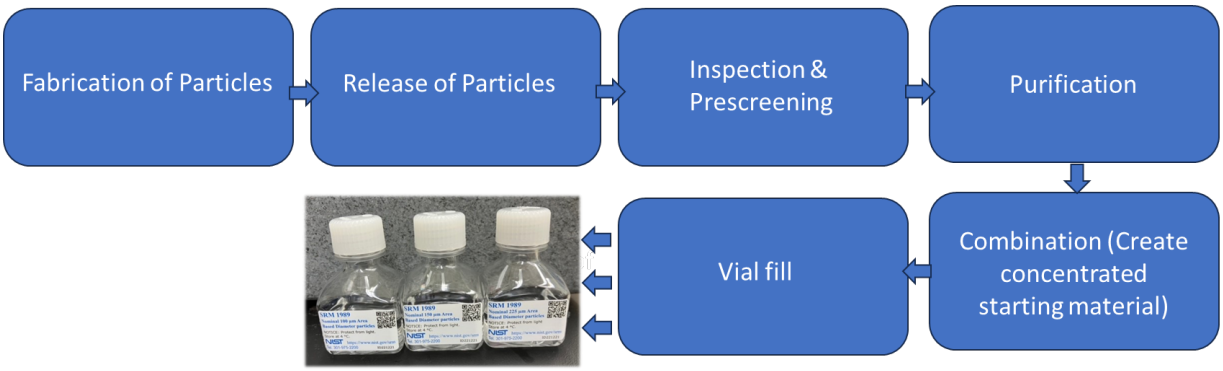

Figure 2. General schematic to produce and fill the vials for SRM 1989

3.1. Formulation

The SRM 1989 particles are suspended in 0.01% (w/v) Triton X-100 (Sigma-Aldrich, St. Louis, MO) and 0.02% (w/v) sodium azide (Ricca Chemical Company, Arlington, TX) in 18 MΩ·cm deionized ultra-filtered water (DIUF). This solution is hereafter labeled Triton diluent. All diluent was prepared in laminar flow hoods using clean, calibrated glassware, balances, and pipettes. The diluent was first prepared at 25 × concentration: 0.25% Triton X-100 (w/v) and 0.5% (w/v) sodium azide, filtered through a 0.1 µm Polyethersulfone (PES) Steritop vacuum filtration unit (Millipore, Burlington, MA), diluted to 1 × and then refiltered to achieve the lowest particle content diluent. Prior to use, filters were washed and particle number concentrations were measured to be low (number concentration N (1 µm)< 100 mL^{-1}) using a DPA 5200 Flow Imaging (FI) instrument (ProteinSimple, San Jose, CA).

3.2. Fabrication of particles

As shown in Figure 3, the fabrication of the particles is composed of 1) coating the silicon wafer with an Omnicoat release layer followed by a layer of SU-8; 2) exposing areas of the wafer to UV light to create the particles; 3) post-exposure baking of the wafer to crosslink the UV-exposed areas; 4) removing unexposed SU-8 (i.e. developing); and 5) dissolving the Omnicoat release layer with a strong solvent and releasing the fabricated particles into the solvent. Each of these steps are briefly described below. In general, the SU-8 processing parameters are available in the manufacturer's datasheets for each of the thickness formulations ranging from 0.5 µm to 150 µm. However, for thin SU-8 films under 5 µm the manufacturer's parameters are only used as a starting point and must be optimized. Table **1** shows some of the optimized parameters used to fabricate the particles applicable to the tools in the NIST NanoFab. Optimal spin speed, exposure dose, time, and temperature for both the soft bake and post-exposure bake, and spinner parameters were determined.

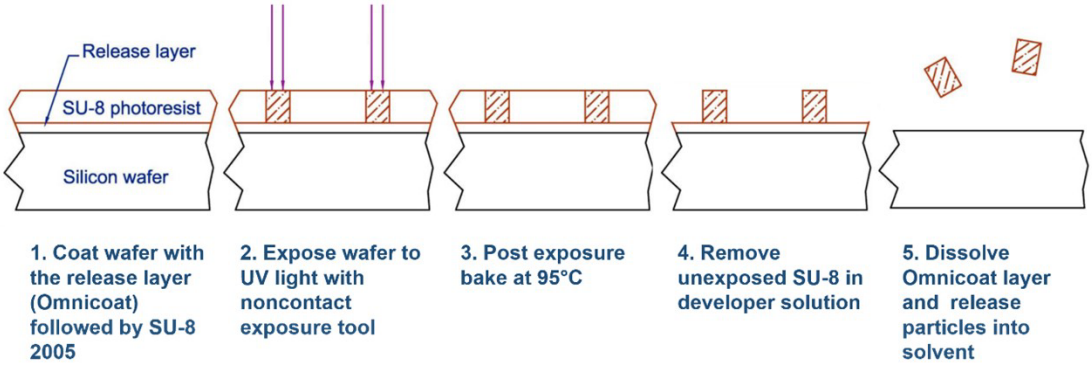

Figure 3. Key steps in the particle fabrication process

Table 1. Optimized parameters for producing the photolithographic particles.

Optimized parameters	
SU-8 formulation	SU-8 2005
Soft Bake	95 ˚C, 3 min (all thicknesses)
Exposure Dose	600 mJ/cm^2 for 220 µm ABD and 150 µm ABD; 800 mJ/cm^2 for 100 µm ABD
Exposure Time	10 min (all thicknesses)
Post Exposure Wait	5 min (all thicknesses)
Post Exposure Bake	95 ˚C, 2 min (all thicknesses)
Particle Thickness	2.5 µm for 100 µm ABD 3.0 µm for 150 µm ABD 3.5 µm for 220 µm ABD
Circular Hole Diameter	4.0 µm for 100 µm ABD 4.0 µm for 150 µm ABD 4.5 µm for 220 µm ABD
Spin parameters	First stage: acceleration = 50 rpm/s for 7 s to spread resist; Second stage: final spin speed = 4000 rpm (100 µm ABD), 3500 rpm (150 µm ABD), 2000 rpm (220 µm ABD); acceleration = 4000 rpm/s for 90 s for all 3 sizes to ensure uniform film thickness

3.2.1. Coating the wafer with Omnicoat and SU-8

Single-sided 4” wafers (purchased from the NIST NanoFab), that have undergone standard RCA cleaning, were prepared by baking them at 200 ˚C on a precision hotplate (Osiris UNIXX HeT20 Tabletop Hotplate, Osiris International GmbH, Germany) for 5 min to remove water and cleaned using a 200 W oxygen plasma for 2 min with a Plasma Etch Tool (Unaxis 790). After the plasma cleaning, 2 layers of Omnicoat (Kayaku Advanced Materials G112850, Westborough, MA) were spun onto the wafer at 1500 rpm using a photoresist spinner (CEE Apogee Spin Coater). To spin on the SU-8, a two-stage spin is used where the wafer slowly accelerates to 350 rpm to spread the SU-8 and then ramps up quickly to the final spin speed. The spin parameters used are described in Table 1. A constant volume of SU-8 (4 mL) was dispensed, without creating bubbles, to ensure a repeatable thickness of the SU-8 layer. A soft bake is necessary to remove excess solvent from the film and allow the wafer to be handled (SU-8 will no longer flow, and the wafer does not need to be kept perfectly level). This was done by removing the wafer from the spinner and baking it at 95 ˚C for 3 min. To prevent contamination of the tools with residual SU-8 remaining on the wafer, it was sometimes necessary to carefully remove any SU-8 on the edge and bottom surface of the wafer with acetone. Uniform hotplate temperature must be maintained, and all the spinning, baking, and handling of the wafers must be done in a laminar flow hood to ensure minimal particle contamination.

3.2.2. Exposing the wafer to UV light

Prior to exposing the wafer to the UV light, the particle design shown in Figure 2, which was designed using LEDIT software and exported into a GDSII file, was uploaded into to the exposure tool (Heidelberg Instruments MLA 150). The wafer was then placed into the tool and the exposure wavelength set to 375 nm. The size of the written area was designed so the exposure time was ten minutes for each of the wafers. The exposure dose used was 800 mJ/cm^2 for the 100 µm ABD particle sized wafers and 600 mJ/cm^2 for the 150 µm ABD and 220 µm ABD particle sized wafers. After the 10 min exposure, during which the instrument wrote the pattern on the wafer, the wafer was allowed to rest for 5 min before the post exposure bake.

3.2.3. Post-exposure bake

The SU-8 crosslinking occurs during the post-exposure bake. The wafer was placed on a hotplate set to 95 ˚C for 2 min. After the bake, the wafer was removed and allowed to cool for 1 min before the unexposed (i.e. not crosslinked) SU-8 was washed off the wafer in the development step.

3.2.4. Remove unexposed SU-8 (development)

After the post-exposure bake, the wafer was submerged in a dish of SU-8 developer (Kayaku Advanced Materials, Westborough, MA) and agitated for 3 min to dissolve and remove the

unexposed SU-8. Upon removal from the solvent, the wafer appeared as a diffraction grating in the light. The wafer was then submerged in a dish of isopropanol (CMOS grade isopropanol) and agitated to remove the developer. The wafer was removed from the dish and sprayed gently with isopropanol and dried with nitrogen. The wafer was inspected under a microscope to ensure the development was completed. The film thickness was measured on a Dektak profilometer and the internal holes were measured using a calibrated inspection microscope at 100 × magnification. The desired film thicknesses and internal hole sizes for each size are shown in Table 1. To remove the remaining solvent on the SU-8 film, the wafer was baked in a vacuum oven at 95 ˚C for 12 h; this low vacuum and heat were used to remove the excess solvent from the film. As with any liquid development of a photoresist, there will always be a very thin (nanometer scale) film left on the wafer. This could cause some of the particles to stick together when released, so a short oxygen plasma etch can be employed to remove this layer (200 W for 45 s). A hard bake at 200 ˚C for 20 min, on a high precision hotplate, annealed the film removing any cracks and decreasing the residual stress.

3.2.5. Defect repair before release (if needed)

The wafer was then inspected under a 5 × objective to see if any defects were present. Despite extreme care during the fabrication process, sometimes contaminants are present. If repair is possible and the damaged area is small, damaged particle could be removed by depositing a single drop of 1165 Remover (MICROPOSIT Remover 1165, Kayaku Advanced Materials) over the damaged area, waiting for 3 h to dissolve the Omnicoat layer, and then washing the area with isopropanol to release the damaged particles. A cleanroom tip wetted with 1165 could also be used to carefully remove a small region of damaged particles as well.

3.2.6. Release of particles

To release the particles, a wafer was placed in a polypropylene jar (Fisher Scientific 02891F) and submerged overnight in a solution of 1165 Remover and a droplet of Triton X-100 to dissolve the Omnicoat and release the particles. The droplet of Triton X-100 was added to prevent particles from sticking to each other during vacuum filtration. This solution was then poured into a vacuum filtration apparatus, which consisted of a collection vessel attached to a polypropylene bottle top vacuum filter funnel assembly with a pre-cleaned and pre-conditioned 0.45 µm polytetrafluoroethylene (PTFE) filter (Foxx Life Sciences, Autofil Polypropylene Bottle Top Vacuum Filter Funnel Assembly, Salem, NH). In this instance, the particles were the retentate; we have used the filter to collect the particles while the solution is the filtrate and is vacuumed into the collection vessel below. This is followed by 3 washes of the filter and retentate with isopropanol to remove any residual 1165 Remover, and then 3 rinses with the Triton diluent to remove the isopropanol. Once washed with the Triton diluent, the particles retained on the filter were harvested by adding approximately 40 mL volumes of Triton diluent and gently swirled to dislodge the particles from the filter. The solution containing the particles was gently removed by pipetting and transferred into a 125 mL polyethylene terephthalate glycol vial (PETG, Nalgene vial with high-density polyethylene closure). The step was repeated until approximately 125 mL of Triton diluent plus particles were harvested into the vial. During

each vacuum step, the filter was kept moist to prevent the particles from sticking to each other. The contents from multiple wafers were not combined at this stage; particles from each single wafer were released into a single vial.

3.3. Inspection and Pre-screening of Particles from Different Wafers

To generate sufficient particles for at least 200 units of this SRM, numerous wafers were processed as described above, for each of the 3 sizes. We needed 4 wafers for the 100 µm ABD, 9 wafers for the 150 µm ABD, and 16 wafers for the 220 µm ABD particles. More wafers were needed as the particle size increased since fewer larger particles could fit on a wafer. We generated more wafers than required since we anticipated that some wafers would contain defects and/or suboptimal particles. It was important that the content of each vial of particles was inspected for physical defects such as excessive curling, bowing, or stuck particles.

Each vial (which contained particles released from 1 wafer) was initially visually inspected by an analyst in front of a black and white background to note for any discrepancies. If a vial contained any visible particles other than the SU-8 particles, that vial was removed from further screening. An aliquot from each vial that passed the initial visual screening was microscopically inspected and particle size characterized as described in more detail in Section 4.2.1. Upon measurement, particles were found to be acceptable for use as an SRM if the standard deviation of the ABD size for particles from that vial was calculated to be below 0.5 %. All the vials that met this criterion were combined and purified to become the starting concentrated batch of the SRM, before the fill.

3.4. Purification of the particles

Particles in the vials that passed both the visual and microscopic screening were of good quality but still needed to be purified to eliminate small subvisible contaminants that cannot be seen by the naked eye. This was done by allowing the sample to settle overnight and by exchanging the diluent with fresh particle-free diluent to remove small particles still suspended in the solution. The large SU-8 particles settled quickly while the small subvisible particles settled much more slowly. This type of diluent exchange, where diluent is gently removed from the container and the same volume of fresh diluent is added, was done 3 times to remove the non-settled, smaller, subvisible particles without disturbing the large, settled SU-8 particles. Flow imaging (FlowCam Benchtop VS1, Yokogawa Fluid Imaging Technologies, Scarborough, ME) was used (with a 300 µm field of view cell at 4 × magnification) to confirm that the small particles were sufficiently reduced.

3.5. Combination of vials

Upon verifying that the vials had a low subvisible particle content (subvisible particle content lower than 50 mL^{-1}), 4 prescreened vials were combined into 1 large vial for the 100 µm ABD particles, 9 prescreened vials were combined for the 150 µm ABD particles, and 16 prescreened vials were combined for the 220 µm ABD particles.

3.6. Vial Fill

Prior to vial filling, a small subset of the 30 mL PETG vials (ThermoFisher Scientific Waltham, MA) were verified for low particle number concentration, generally less than 100 mL^{-1} in the size range between 1 µm ≤ diameter, d ≤ 20 µm. These vials were used for SRM packaging. Earlier stability studies indicated that these vials (among other vials tested) were optimal storage vials for the diluent and particles used for this SRM. The diluent was also checked for low subvisible particle content (number concentration < 50 mL^{-1}).

Three separate fills were performed in-house, one per particle size. Each fill was performed manually in a laminar flow hood in an assembly-line fashion. Each of the 210 vials was filled with 1 mL concentrated particle suspension followed by 19 mL of the diluent to achieve approximately 20 mL of sample in each vial with a particle number concentration of approximately 100 mL^{-1}. The caps were initially tightened, and then were tightened further after several months to ensure secure lids.

4. Characterization of SRM 1989

SRM 1989 delivers a certified value for particle size. Particle number concentration is a value of interest to the end user that would help with sample handling and use. The characterization of the SRM for these values (see Figure 4) will be described in this section.

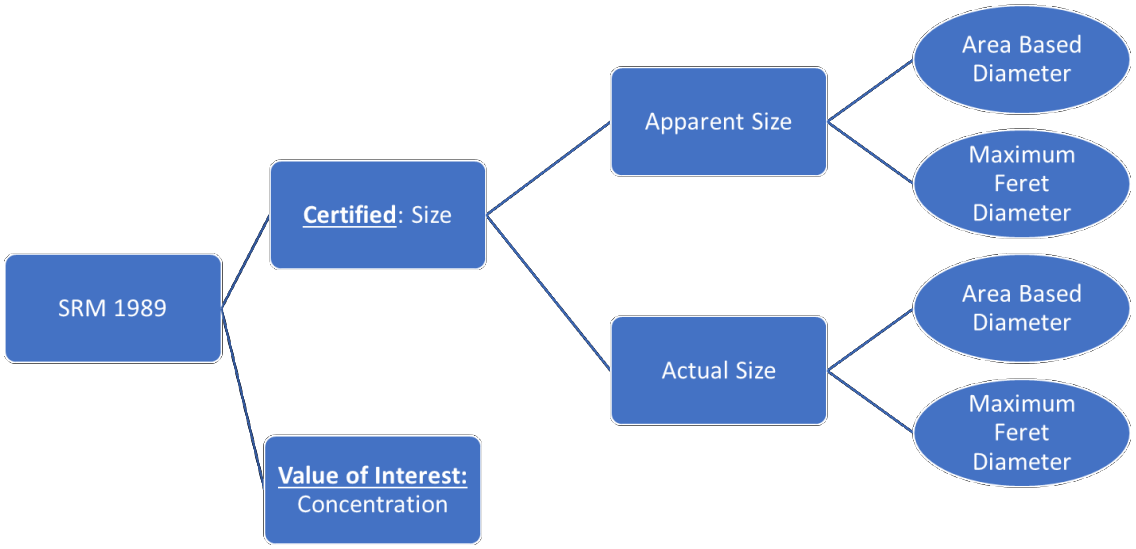

Figure 4. Schematic showing the characterization values for SRM 1989 for of the certified size values and for particle number concentration (the value of interest).

For particle size determination, a procedure was developed using optical and scanning electron microscopy to determine the apparent and actual size, and the related uncertainties. Apparent size is the experimentally determined size from optical measurements at a numerical aperture of 0.30. The actual size, or the true diameter of the particle, was determined by correcting the apparent size for optical diffraction effects. The SRM certificate reports values for both Area Based Diameter (ABD) and Maximum Feret Diameter (MFD) for each particle size. ABD is the diameter of a circle with the same number of pixels as a particle in a binary image. MFD is the maximum distance between two parallel planes touching a particle border but not intruding into the particle interior. These certified dimensional values are traceable to the Standard Meter through the use of a NIST-calibrated stage micrometer, which provides a length reference that is traceable to the SI.

For particle number concentration determination, a procedure was developed using an optical microscope to determine the particle number concentration of the concentrated SU-8 solution. A modified procedure was developed to determine the particle number concentration of the final filled, aliquoted vials.

4.1. Particle number concentration determination

To perform a uniform fill in which each vial contains nominally 100 mL^{-1}, it was necessary to determine the number concentration of the starting solution as well as understand the settling behavior of the particles. To measure the number concentration, a known amount of sample (determined gravimetrically) was loaded into a Palmer Chamber (PC) reservoir (Electron Microscopy Sciences, Hatfield, PA) and imaged under a microscope at 5 × magnification. The complete sample was scanned manually by rastering across the area of the containing well and counting all particles observed with a tally counter. Separate experiments were conducted to understand particle sedimentation and resuspension.

4.1.1. Methods

Particle number concentration in the concentrated solution (pre-fill and post-fill)

The particle number concentration in the concentrated sample was determined prior to filling the vials (pre-fill) and after filling the vials (post-fill). First, the sample was resuspended using a 10 mL pipet to draw up 5 mL of the sample and then expelled back into the sample bottle. This was done a total of 10 times to ensure complete mixing and will be referred to as 'pipette mixing' throughout this document. Then, a 1 mL pipette tip (with a 0.4 cm cut off tip) was used to extract 0.1 mL well-mixed sample and placed into a PC reservoir that holds approximately 0.1 mL of liquid for viewing using a microscope. The exact amount of sample for use in the concentration calculations was determined gravimetrically by weighing the PC before and after sample placement. The PC was placed in a Leica DMRX brightfield microscope (Leica Microsystems, Wetzlar Germany) and viewed under 5 × magnification with a viewing area set to a width of 2.0 mm. After the particles have settled, the 2 mm wide viewing area is translated vertically across the PC, while particle observations are recorded manually using a tally counter. Once the first vertical swath has been counted, the viewing area is translated horizontally by 2 mm and the next vertical swath is counted. In this way, the viewing area is rastered across the entire area of the PC, and all particles are counted. To help ensure that particles on the edges of the viewing are counted accurately, particles contacting the left edge of the viewing area are counted but those contacting the right edge are not. In addition, for better precision and accuracy, a second measurement of the same sample well was made, but with the sample starting position being shifted horizontally by 1.0 mm. The two counts were then averaged for a total count per volume (assuming density of water to be 1 g/mL).

Particle number concentration in the aliquoted sample vials

To measure the particle number concentration in the filled vials, 3 vials were randomly chosen with one vial from near the beginning of the fill, one from the middle, and one from the end. The particle number concentration (mL^{-1}) present in these aliquoted sample vials was determined in a similar manner as was described for the concentrated solution. The number particle number concentrations in these samples was nearly twenty times more dilute than the initial concentrated samples. As a result, the PC used for the concentrated solution measurements was not suitable as it could not accommodate the high sample volumes

required for these samples. Therefore, we used a chambered coverglass system (Cellvis, Mountain View, CA) with 4 wells, each with dimensions of 9.3 mm wide × 19.9 mm long × 10.8 mm deep, with each well capable of holding 2.0 mL in volume. To measure the particle number concentration in these samples, two aliquots of known mass (around 1.5 mL) were placed in two wells of the 4-chambered well system mounted on a microscope slide. The mass of the aliquoted volume was determined gravimetrically. Particles were allowed to settle, and then deionized water was added to fill the two wells just slightly above the brim, after which a 20 mm × 30 mm coverslip was placed over the wells. Samples were allowed to settle for 5 min before counting, until they appeared in a uniform focal plane. Particles were observed and counted in a similar manner as for the concentrated solution (above), while recording the particles in each well separately. The counts from the two wells were then combined into a total count per volume of both aliquots. To verify the counting, as described above for the concentrated solution measurements, a second count of the same two wells was performed after translating the initial position by 1 mm. From the recorded data, the average number concentration was calculated by dividing the total count of both wells by the weighed mass of the sample in both wells, as determined gravimetrically prior to the addition of deionized water to top off the wells. Each sample was measured in this way at least twice (three times in most cases).

Settling and Resuspension

To ensure uniform aliquoting of the concentrated samples during the fill, it was necessary to determine the optimal resuspension conditions. To achieve this, we conducted a study to determine how long it takes for the particles in the 220 µm ABD sample to settle to the degree that a reduction in concentration was observed in the measured aliquots. To determine the settling rate, the sample was first resuspended by shaking and then waiting an hour with periodic gentle tumbling to allow the foam to subside. Prior to starting the timer, the sample was resuspended by pipette mixing, as described above. Immediately after mixing, a timer was started and the container sat without being disturbed until an aliquot was extracted and placed in the PC for concentration measurement. Settle times investigated included 0 s, 30 s, 60 s, 90 s, 120 s and 180 s (Figure 5). Ten measurements were made for the 0 s timepoint. At each of the later time points, 4 measurements were obtained, except for the 180 s timepoint where there were 3 measurements made. Each time a measurement was made, the sample was resuspended by pipette mixing, and the timer was reset, so the measurements were independent of one another.

When comparing the settling rate of the 220 µm ABD particles over time, as displayed in Figure 5, no drop in concentration is observed up to 60 s settle time. At 90 s, a mild reduction is observable which becomes more pronounced at 120 s and 180 s. Considering this, it was determined that 60 s between resuspensions is sufficient to maintain fully suspended particles for the 220 µm ABD concentrated solution. The knowledge of the settling behavior was used to determine how many vials could be filled with 1 mL aliquots of the concentrated starting solution before resuspension is required. It was determined that when there is over 100 mL of sample in the 250 mL container, pipette mixing ten times every 60 s during aliquoting and

extracting the sample from near the middle of the solution is sufficient. As the concentrated solution volume becomes lower than 100 mL, swishing the solution between each aliquot and still extracting the aliquot from the center of the solution becomes necessary to keep the particles sufficiently suspended to see uniformity in the aliquot concentration. We determined that extracting accurate aliquots from a solution lower than 50 mL makes it difficult to draw uniformly suspended aliquots. A more detailed analysis of the results is not necessary at this point since this study was performed to identify the settling trend that would enable us to determine the filling protocols. These measurements were made on the 220 µm ABD particles, which should settle more quickly than the smaller sized particles. Therefore, we deemed that the protocol for the largest particles was at least good enough for the remaining two smaller particle sizes.

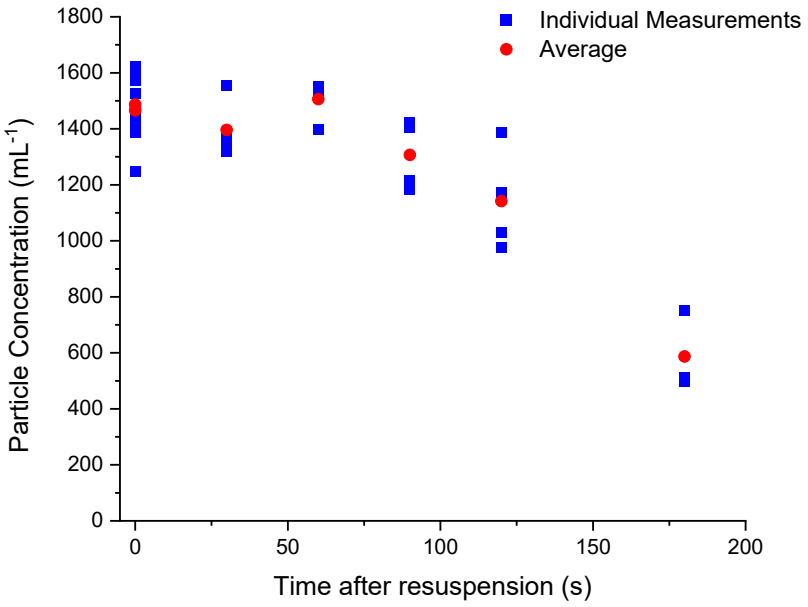

Figure 5. Settling time of 220 µm ABD particles after resuspension

4.1.2. Results

Particle number concentration in the pre-fill vs. post-fill concentrated solution

Table 2 compares the particle number concentrations of the concentrated solution pre-fill and post-fill, as well as the concentrations of the aliquoted sample vials. For all three sizes, the particle number concentration of the concentrated solution is higher post-fill compared to pre-fill. There are several potential mechanisms for this phenomenon. Sedimentation occurs during aliquoting after each resuspension of the particles. If the aliquots are taken from a position within the initial sample volume that has experienced a decreased concentration due to sedimentation, then the concentrated particle solution would become more concentrated over time. There are other potentially more subtle and possibly competing factors, such as entrainment of particles that could occur as the aliquot volume is drawn up into the 10 mL pipette due to shear effects that could either result in particles being pushed away from the pipette tip or aspirated in. Note that during the fill, 1 mL aliquots are taken with a 10 mL pipette tip, which has a larger tip opening as well as a higher sample volume than the 1 mL pipette tip, which was used to sample 0.1 mL samples for the concentration measurements. The 1 mL pipette tip was cut off to obtain a larger opening, but the shear effects could be very different between these two withdrawal conditions. It is also possible that with the low solution volume of the final concentrated solution, it was difficult to obtain a 0.1 mL volume sample that was representative of a uniformly well-suspended solution, due to spatial variations in solution concentration and sedimentation. For the 100 µm ABD particles in Table 2, the initial concentrated solution is measured to be 46.7 % more concentrated after all aliquoting has been completed. In the 100 µm ABD aliquoted samples, no monotonic increase or variation is observed throughout the fill for the vials observed. However, for both the 150 µm ABD and 220 µm ABD aliquoted samples, the number concentration is observed to increase during the fill, albeit substantially less than the increase that is observed for the initial concentrated solution measurements. For instance, the number concentration for the aliquoted 150 µm ABD particles increases by 16.6 % throughout the fill, as compared to the 28 % increase in the concentrated solution. Likewise, the number concentration for the aliquoted 220 µm ABD particles increases by 8.5 % over the course of the fill, compared to the 22.0 % increase of the concentrated sample.

It appears that a fortuitous set of competing factors has resulted in less variation in the number concentration of the aliquoted samples over the course of the fill compared to the starting concentrated solution with aliquoted number concentrations in the range of 100 mL^{-1} which do not vary substantially over the course of the fill. Note that the potential issues with shear as well as particles being restricted from entering the pipette tip are not expected to be a strong factor during concentration measurements of the aliquoted samples due to the higher (× 30) sampling volume of two 1.5 mL withdrawals and the larger pipette tip opening using the 5 mL pipette tips.

Table 2. Particle number concentration measurements for concentrated particle solutions pre-fill and post-fill and for the individual vials after being filled. SD represents standard deviation. Each measurement is the average of at least 3 measurements; SD represents standard deviation.

	Pre-Fill (concentrated solution)	**Post-Fill (concentrated solution)**	**% Change**	**Aliquoted Vials**			
Nominal Particle Size (µm, ABD)	Particle Number Conc. ± 1 SD, (mL^{-1})	Particle Number Conc. ± 1 SD, (mL^{-1})	Post-fill vs Pre-fill of starting vial	Vial #	Particle Number Conc. ± 1 SD, (mL^{-1})	Average Particle Number Conc. ± 1 SD, (mL^{-1})	% change (from first vial)
100 µm	1567 ± 82	2299 ± 160	46.7%	11	109 ± 5	111 ± 5	
				112	117 ± 2		8.0%
				190	108 ± 1		-0.3%
150 µm	1471 ± 144	1883 ± 139	28.0%	9	92 ± 6	99 ± 8	
				109	98 ± 1		6.5%
				189	107 ± 6		16.6%
220 µm	1556 ± 48	1901 ± 252	22.0%	6	91 ± 8	94 ± 4	
				109	93 ± 6		2.6%
				183	99 ± 13		8.5%

4.2. Particle Size of SRM 1989

To measure particle size, 2 optical microscopes (Microscope 1 and Microscope 2) and 1 scanning electron microscope were used. The sizing data acquired from the two optical microscopes were used to evaluate the optical (or apparent) size of the particles as well as the various sources of uncertainty. Microscope 1 was used primarily for determining the particle size, lot homogeneity, and stability of particle size. Microscope 2 was used to confirm and complement the first method's data and for uncertainty analysis. Scanning electron microscope (SEM) data, along with mathematical corrections to the apparent size of the particles, were used to correct for the diffraction effects of particles and provide the "actual" or true size of the particles. Size data (both apparent and actual) are represented in terms of Area Based Diameter or Maximum Feret Diameter.

Microscope 1 (Leica Microscope) is an upright microscope where the objective is above the stage so it images from above the sample, through the liquid sample and cover slip. Microscope 2 (Zeiss Axio Observer Z1, Carl Zeiss USA, Thornwood, NY) is an inverted microscope with the objective located below the stage so it images through the bottom of the sample. Both microscopes were used with a green light source, and a 10 × objective with 0.3 numerical aperture (NA). Images of the background and stage micrometer were collected prior to collecting the particle images on each day of data collection. These images were used for background correction or for converting pixels into micrometers, respectively, using Excel and Fiji image analysis software (9). Prior to starting the data analysis, the camera for Microscope 1 was assessed to screen for camera sensor defects. Data acquired with Microscope 1 was also used to assess for homogeneity of the lot and size stability of the particles.

While the SRM is not explicitly a morphology standard, some morphological parameters were automatically acquired during the data acquisition. These values, which do not fall under NIST's categorization of certified, non-certified, or "value of potential interest," will be briefly described. It must be noted that, since these morphological values have not undergone the same stringent statistical testing as was done for particle sizing and particle number concentration, to an extent, they do not represent any official values associated with this SRM.

4.2.1. Apparent Size

To determine the apparent size of the particles, a representative set of vials from each size range were characterized for particle size using the two optical microscopes and the data were analyzed using Fiji.

4.2.1.1. Methods

Microscope 1

Approximately 120 µL of a well-mixed sample solution containing the particles from 1 vial were injected into a pre-cleaned and dried glass PC, without forming any air bubbles. The particles that settled on the bottom of the glass chamber were imaged using a Leica microscope with an Andor Zyla 5.5 (Oxford Instruments, Abingdon, UK) or CS235MU Kiralux Camera (Thorlabs, Newton, NJ) with the zoom setting on the microscope-to-camera adapter set at 1.25 ×. A stage micrometer image was collected at the beginning of each day to allow calibration for the image pixel size. Köhler illumination was adjusted while imaging the stage micrometer and then on the first image of the sample to obtain even illumination of the images. Before analysis, image files were cropped to remove particles that were dirty, in poor focus, or excessively bent so they do not affect the calculations. At the start of each day, 5 background images of the chamber (without particles in view) were collected. For each vial, at least 8 images were collected per analyst. The images were autosaved and stored for analysis with Fiji software. The five background images were read in Fiji and converted to a stack. The median of the five images at each pixel location was created by using the median projection and saved as the median background image.

A macro was written and saved as an IJM file to do the following steps 1 to 7:

1) Open the saved particle images and convert them into a stack
2) Crop the file as appropriate for the camera used to collect the image.
3) Divide each image in the stack by the median background image.
4) Normalize the image intensity to give a median pixel intensity of 2000.
5) Convert the file to a binary image by applying a threshold (nominally 1545, but this can be reset).
6) Fill the holes in the binary images.
7) Measure the particle size and area of the binary images.

After step 7, the images were thresholded to nominally 1545, as that was determined optimal for these particles from previous studies. However, this is not the final threshold used; manual analysis of the resulting output images from this first thresholding was performed to find the threshold value that best corresponds to the midpoint between the background intensity (set at 2000 by the normalization) and the intensity of the dark center of the particle border. This midpoint intensity threshold is recommended by ISO 13322-1:2014 (10). This manual analysis of the output images was done by opening the normalized file produced by the macro in Step 4 above and scrolling through each image. The threshold for each frame on this image was manually adjusted so that only 50 % of the periphery of the particle (not the circles within the particle) was below the threshold. This can be quite subjective, so a representative image of a particle set to this threshold is shown below in Figure 6. Finding the point of 50 % detection of the border approximately corresponds to finding the mean intensity value of the dark center region of the particle border. These threshold values for each image in the stack were recorded. The thresholds determined for each image were then averaged together and then further averaged with 2000 (which is the background intensity), to determine the new threshold corresponding to the intensity halfway between the background and the darkest part of the image borders. This

new calculated threshold value was entered into the macro and rerun. Therefore, the macro was run twice; on the first macro run, the first threshold was used to normalize the images, and on the second macro run, the calculated threshold was used to provide the corrected particle sizing information.

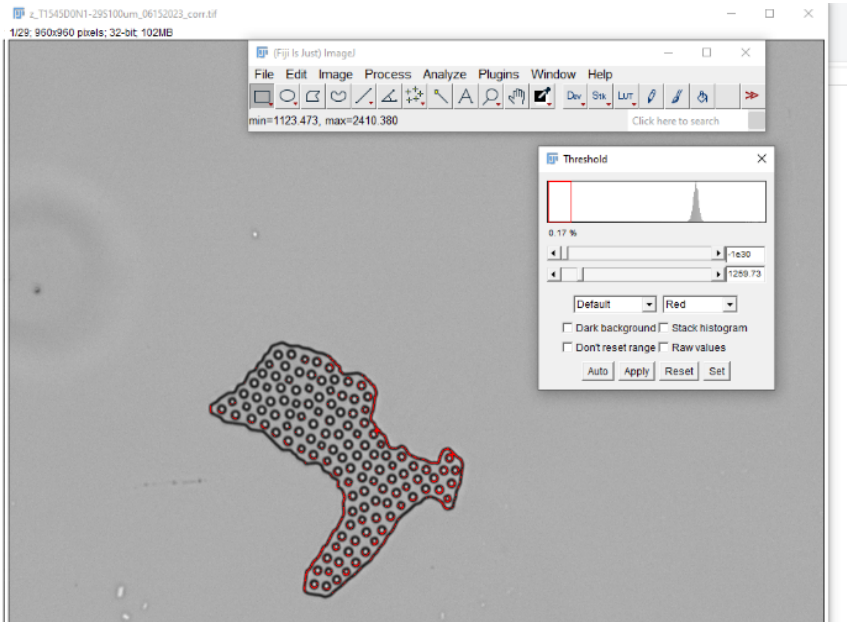

Figure 6. Representative image of a particle where the threshold is set so the outer border of the particle is approximately 50% complete (shown as red pixels).

Either before or after the thresholding, as was described above, it was necessary to determine the dimensions of the image pixel using the calibrated stage micrometer. This was done by opening the stage micrometer images and comparing the distance in pixels between rulings on the NIST-calibrated stage micrometer to the certified distance values in micrometers. The distance between rulings was obtained from an intensity profile of the gray-scale image by finding the pixel locations corresponding to the intensity value halfway between the background intensity and the intensity at the center of the ruling. Calibration of the pixel image size is necessary to convert ABD and MFD values measured in pixels to micrometers. The pixel size for each day of acquired data was obtained from a stage micrometer image acquired on the same day.

Microscope 2

Microscope 2 data were not used for the certified size value assignment but to provide independent particle size measurements that can be compared with Microscope 1 results. This approach was used to validate and determine the uncertainty associated with the measurements. With this second method, a much more limited number of particles were analyzed.

Different SRM vials than the ones used for Microscope 1 were used for analysis. A similar set up as Microscope 1 was used for Microscope 2. A green LED (centered at 530 nm, exposure 100 ms, at 4

μW intensity, Thor Labs LED M530-L4-C4) was used. Neutral density filters (Edmund Optics, Barrington, NJ) were used to reduce intensity of light from entering the 16-bit camera to obtain a more stable output. As with Microscope 1, a 10 × objective with 0.3 NA (numerical aperture) was used. A total of 3 vials were measured; 1 vial for each particle size, fewer vials than what were used for Microscope 1. The measurements were performed by a single analyst on the same day.

One major difference with Microscope 2 compared to Microscope 1 is that it can take automated images of particles at different focal planes, or z-stacks, and the image of best focus was determined from inspection of the images. Here a z-stack of 30 was used and exposure time set to 100 ms. An additional difference was that the particle solution was imaged from below through a glass-bottom well plate.

A 6-well, glass-bottom plate (Cellvis, Mountain View, CA) was tared before a well-mixed sample solution (gently swirled 10 times) of a particle sample was loaded into a well using a pipette with a trimmed pipette tip. The sample aliquot was pipetted from the bottom ⅓ of the vial. This approach was repeated for each of the six wells, with two wells allocated to each particle size.

Approximately 20 particles in the well, for each size, were manually selected and their coordinates provided to the software. Rather than taking one image with the particle in focus, a stack of 30 images at different focal planes (approximately 1 μm apart in the z-direction) for each particle were imaged. Images of the stage micrometer and five background images, containing no particles, were also collected.

Image analysis was performed similarly as was done with Microscope 1 data, with some small differences. For analysis of the data, even though 30 z-planes for each particle were collected, we only used 4 z-planes for each particle. We selected 4 planes that were closest to the optimal focal plane of the particle. This was done manually by looking at each frame in the combined stack in Fiji and noting in which frame each particle had the sharpest edges. The other 3 z-planes selected were directly above or below the optimal z-plane chosen. Unlike with Microscope 1, which had a uniform intensity in the background, the images from this microscope sometimes displayed an intensity gradient in the background moving from the left to the right of the frame (likely resulting from optical effects near the edge of the well). To make sure that the gradient difference was not too large, we had to review each frame and check that the background intensity close to particles on all sides was within the intensity range of 2000 pixels ± 30 pixels; if they exceeded this intensity, the images were not included in the analysis. Similarly, images were viewed to identify the 50 % median threshold as was done with Microscope 1. Since the 4 frames for the identical particle(s) are similar, the intensity threshold should be similar for each of the 4 frames. Out of the four z-planes, one was manually selected by an analyst for final sizing analysis based on how well the particles were in focus in that chosen plane. This was then compared to the result obtained with Microscope 1.

4.2.1.2. Results

The sizing values described in this section represent the apparent particle size obtained from Microscope 1. To gain a better understanding of how the microscope itself can impact the sizing measurements, Microscope 2 was also used to measure the 3 particle sizes. While this second measurement was not used to determine the certified values, we used the variation of size measurements between the different microscopes to understand the level of variability due to the instrument and incorporate it into the uncertainty analysis. Note that the apparent size will vary if the particles are measured in systems with different optical resolution than the 10 ×, 0.30 NA systems used in the present study (see Figure 8 and related text for results on the dependence of size on NA). All the sizing data were analyzed similarly using Fiji.

Using Microscope 1, approximately 200 particles of each of the three sizes were imaged and measured. The average size, standard deviation (SD), relative standard deviation (RSD), and experimental standard deviation of the mean (ESDM) are shown for both the ABD and MFD measurements in Table **3**. The small SD and RSD indicate that the particles are very homogeneous in terms of size, and well within what the user community requires. On Microscope 2, a much more limited number of particles were analyzed. Those results are shown below in Table 4.

Table 3. Apparent size of the 3 size ranges of SRM 1989, from Microscope 1.

Nominal Particle Size (µm)	# of Particles Analyzed	ABD (µm)	SD (µm)	RSD (%)	ESDM (µm)	MFD (µm)	SD (µm)	RSD (%)	ESDM (µm)
100	198	100.65	0.47	0.47	0.03	149.11	0.46	0.31	0.03
150	199	150.16	0.53	0.35	0.04	223.08	0.53	0.24	0.04
220	172	222.39	0.41	0.18	0.03	333.33	0.58	0.17	0.04

Table 4. Apparent size of the 3 size ranges of SRM 1989, from Microscope 2, on a limited number of particles.

Nominal Particle Size (µm)	# of Particles Analyzed	ABD (µm)	SD (µm)	RSD (%)	ESDM (µm)	MFD (µm)	SD (µm)	RSD (%)	ESDM (µm)
100	16	99.91	0.41	0.41	0.10	148.80	0.42	0.28	0.11
150	25	149.04	0.57	0.38	0.11	222.47	0.74	0.33	0.15
220	12	222.27	0.34	0.15	0.10	333.58	0.30	0.09	0.09

In a separate experiment, see Section 4.2.2, 5 particles of each size were imaged on gold-coated slides (Table 5). This experiment was performed to see if particle mounting on a different surface can lead to differences in optical image size, even if all other factors are kept constant. Although

this third set is limited in scope, it is valuable in assessing bias between optical setups.

Table 5. Apparent size of the 3 size ranges of SRM 1989 mounted on gold-coated slides, from Microscope 1 but on a limited number of particles.

Nominal Particle Size (µm)	# of Particles Analyzed	ABD (µm)	SD (µm)	RSD (%)	ESDM (µm)	MFD (µm)	SD (µm)	RSD (%)	ESDM (µm)
100	5	98.98	0.38	0.38	0.17	148.25	0.40	0.27	0.18
150	5	148.13	0.71	0.48	0.32	222.19	0.83	0.38	0.37
220	5	221.81	1.39	0.63	0.62	333.45	2.27	0.68	1.02

For the application of visible particle inspection, the differences observed in the 2 microscopes and 3 set-ups are indistinguishable and unimportant. A visual inspection analyst will not be able to differentiate between a 100.65 µm particle versus a 98.98 µm particle. While the optical differences between a standard optical microscope (upright) and an inverted optical microscope are primarily due to their configurations, their resolving power is nominally identical (since both used NA = 0.30 objectives, the same detection wavelength, and Köhler illumination) and we would not expect to see a significant difference between Microscope 1 and Microscope 2 based solely on the microscope illumination and detection.

It is interesting to note here that there was a consistent trend in the sizing of the particles depending on the background medium and microscope used, albeit on the scale of 1 µm. Consistently, the results from Microscope 1 with the particles on the gold-coated slide were smaller in all sizes, in terms of ABD, compared to the other two instrument set-ups. At the largest particle size (220 µm), the variability in the ABD and MFD measurements with the gold-coated slides was larger, most likely due to the very low number of particles used for analysis. The particles on a gold-coated surface had sharper borders, so had a smaller optical size. The exact optical reasons for this are not well understood. Additionally, if we look at the trend, we will see that the results from Microscope 1 for particles in the PC are consistently higher in every size category compared to the results from Microscope 2. The variabilities expressed for both measurements are roughly the same. Again, this difference is not large but an interesting observation. Overall, the uncertainties obtained among the three set-ups are very minimal for the visible inspection application and would not impact the user in how they use these particle standards.

While not presented in detail here, we conducted another study where we looked at the impact of the analyst's selection of the optimal focusing plane and how that impacts the particle size. The study found that the optimal focusing settings among the five analysts were consistent, with results that were within 1 µm of each other. This variation corresponds to about 0.01 µm to 0.14 µm ABD depending on the particle size (from 100 µm to 220 µm ABD).

4.2.2. Actual Size

When objects are imaged in an optical system, the object edges can appear blurry due to parts of the object being out of focus or due to diffraction effects. Both the depth of field (the distance along the optical axis where objects remain in good focus) and diffraction effects depend on the numerical aperture, which is a measure of the size of the light cone collected from the sample by the imaging system. Larger numerical apertures give reduced diffraction effects, but less depth of field.

Because SRM 1989 particles are intended for use primarily with optical systems, we report an apparent size of these particles that includes the diffraction effects. However, the user may benefit by knowing the true size of the SRM 1989 particles. For these particles imaged with a 10 × objective with a 0.3 numerical aperture, the apparent size is a few percent larger than the actual size. In the sections below, we describe measurements of the difference between the true size and the apparent optical size for the SRM 1989 particles. It is shown later that the apparent size of the particle is larger than the actual size because of optical diffraction effects.

While we do not directly measure the actual size, we determine the correction to the apparent size. We do this by four experimental methods (here defined as Models 1 through 4) to measure the difference between the actual and apparent ABD and MFD. The first two models are based on optical analysis. The last two models are based on analysis and comparison of the same particles imaged by scanning electron microscopy (SEM) and optical microscopy. Briefly, we describe the assumptions of each of the models below:

- Model 1 (Optical Border): In this model, we assumed the midpoint of the optical border is a reasonable estimate of the actual particle edge. Therefore, we seek to find an ABD corresponding to a particle boundary located at the middle of the border. This method was employed to calculate the apparent particle size in Section 4.2.1.

- Model 2 (Optical 1/NA Extrapolation): In this model, we assumed that optical resolution theoretically scales as 1/NA, where NA is the numerical aperture of the objective. By plotting the optical (measured) size versus 1/NA, we determined the *y* intercept, which is an estimate of the size at infinite resolution.
- Model 3 (SEM-Optical Area): In this model, we measured the same particles on an optical microscope and an SEM, with an assumption that the SEM gives the actual particle size. The difference in size between the optical and SEM images represents the difference between the apparent optical diameters and the presumed actual (i.e. SEM) diameter.
- Model 4 (SEM-Optical Border): In this model, we measured the distance between the particle edge and adjacent holes for the two methods with the assumption again that the edges provided by SEM are representative of the actual particle edge.

In acquiring these data, we have emphasized obtaining four largely independent results rather than obtaining highly precise data for a single method. This approach is motivated by the observation that all four methods have some degree of unknown systematic uncertainty, and the abundance of models helps us to understand the degree of systematic uncertainty.

4.2.2.1. Methods

For Model 1, no additional samples or experiments were needed. Prior images collected on Microscope 1 for homogeneity assessment were analyzed in an alternate way, as described in Section 4.2.2.2 below.

To prepare samples for Model 2, the SU-8 particles were lightly glued down in the following manner:

- Drop cast a dilute shellac-in-methanol (1 part shellac to 250 parts methanol) solution onto clean slides to give a shellac coating of a few 10 s of nanometers.
- Capture SU-8 particles on a mesh filter, and rinse with both water and methanol to clean particles of surfactant and sodium azide in the diluent.
- Invert the filter, resuspend the particles with a small amount of methanol, and then touch the wet filter bottom to the slide.
- Allow the slide to dry in air in a laminar flow hood.

Five particles of each size were glued onto a glass microscope slide. Each particle was imaged at three different numerical apertures (10 × (0.3 NA), 20 × (0.45 NA), and 40 × (0.55 NA) air-spaced objectives with collars of 20 × and 40 × adjusted for optimum image; green light, Köhler illumination). The camera zoom was adjusted so that each particle size would fit into the field of view for all magnifications. Each particle was measured three times, with the particle position in the field of view slightly altered and the particle refocused for each replicate.

To prepare samples for Models 3 and 4, the samples were prepared in the following manner. First, about 70 nm of gold was evaporated on precleaned 2”× 3” glass microscope slides using an e-beam evaporator. Five SRM SU-8 particles, from each of the 3 sizes were then glued down onto the gold-coated slides with a thin layer of shellac. These gold-plated microscope slides with SU-8 were imaged on the optical and electron microscopes.

Optical images were obtained with the same settings as were described in the apparent size section (Section 4.2.1), with only two differences:

- the light intensity was increased, to compensate for the reduced transmission through the gold, and
- because the gold film has visible intensity variations, 10 background images were acquired instead of the 5 used for the apparent size measurements. Additionally, the background had noticeable horizontal bands, so on acquiring the background images, we

were sure to vary the *y*-axis setting to effectively average out these bands. Finally, the backgrounds were given two Smoothing operations in Fiji.

For electron microscope measurements, a TESCAN MIRA3 Schottky Field Emission Scanning Electron Microscope (s/n MI079107) with an Everhart-Thornley secondary electron detector and a YAG backscatter detector was used. Five images were collected for each of the three samples prepared above to give a total of 15 images; these particles had previously been measured by optical microscopy. The particles were imaged using a beam energy of 15 keV and a dwell time of 100 µs/pixel. Simultaneous 2048 pixel × 2048 pixel secondary electron and backscattered electron images were collected from each particle. For the 100 µm ABD, a nominal 170 µm field-of-view was used. For 150 µm ABD, a nominal 250 µm field-of-view was used. For 220 µm ABD, a nominal 400 µm field-of-view was used. These fields-of-view are measured relative to the nominal instrument calibration which is estimated to be accurate to better than 5 %.

To provide dimensional traceability, additional images of the Geller MRS-4XY s/n R23-104 dimensional reference standard were collected. To maintain the length scale, the image parameters were not changed between acquiring the particle image and the MRS-4XY image. The focus was maintained using the z-axis of the stage. Traceable dimensional calibrations better than 1 % can be extracted from these images. The Geller MRS-4XY s/n R23-104 has been made traceable to the SI through calibration against the NIST Line Scale Interferometer. The calibration report is available as NIST Test No. 821/276683-08.

Separate studies were conducted to check the equivalence of optical and SEM length measurements, using a separate Geller MRS-6XY dimensional reference standard. Comparison of the optical and electron microscopy measurements of the Geller MRS-6XY for both a 1 µm pitch pattern and a 2 µm pitch pattern showed that the two measurements were not statistically different at a 95 % confidence level. Deviation of the two methods was within ± 0.35 % for the 1 µm scale and ± 0.12 % for the 2 µm scale on the Geller.

4.2.2.2. Results

Here we summarize the results of each of the four independent models for the difference between actual and apparent sizes.

Model 1: Optical Border

Skene reports that a comparison of optical and SEM images of polystyrene spheres, for different sphere sizes and refractive index liquids for the optical microscopy, showed that the midpoint of the border accurately matched the sphere diameter when the ratio of the refractive index of particle to liquid was approximately 1.08 (11). In our case, SU-8 in water has a ratio of approximately 1.6/1.33 = 1.2 and we are imaging plates instead of spheres, so the midpoint of the optical border is a reasonable estimate of the actual particle edge, but not definitive.
For our particles, we seek to find an ABD corresponding to a particle boundary located at the middle of the border. This is done by first finding the change in the area of the optical images that corresponds to shifting the particle boundary from the outside of the particle to the middle of the

border. We do this by analyzing the particles in two ways: first with the unfilled particle image to find the border area, and then with the thresholded image filled in to get the total area (see Figure 7).

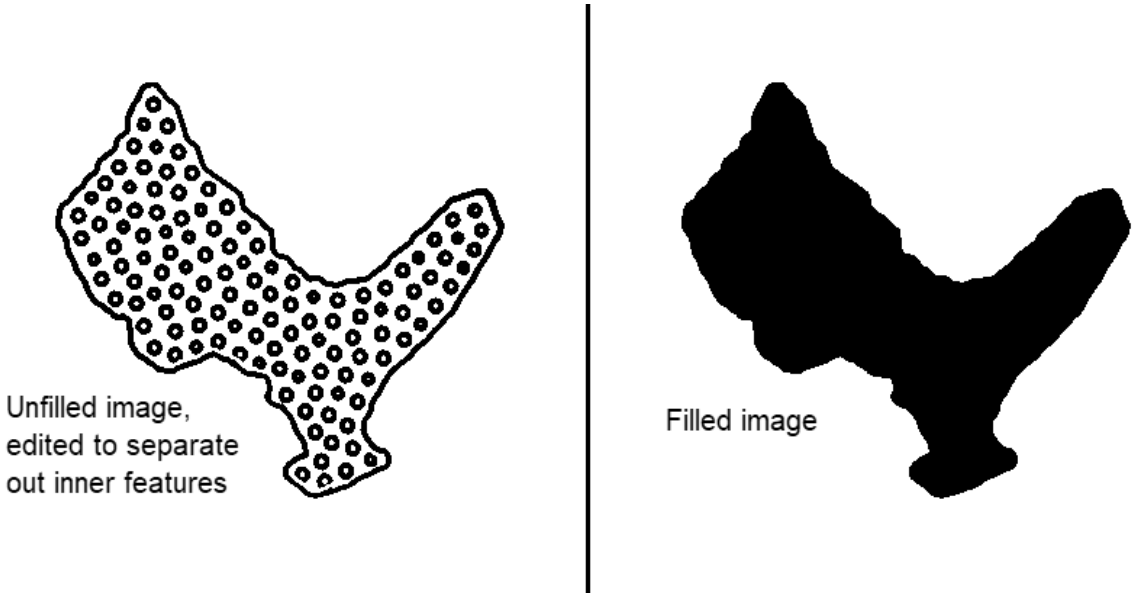

Figure 7. Thresholded particle images obtained by optical microscopy . (Left) Image without a Fill operation, and with any connections of interior features to the border severed; (right) image after a Fill operation.

The change in particle area on moving from the outside border to a line midway in the border is approximately one half of the total border area. This change in area can be expressed as a change in equivalent ABD. Optical effects for some particle geometries could make the border thicker, so this model may give too large a change. This is a Type B uncertainty that is hard to quantify. Nonetheless, this method is a likely upper limit on the magnitude of the ABD change. This method is easy to implement and quite precise.

Mathematically, with A_b the area of the border (i.e. the pixels in the thick black line on the outside of the particle) and A_f the area of the filled image, the relation between the actual and apparent optical ABD is:

$$\mathbf{[1]} \qquad \mathbf{ABD_{act} - ABD_{opt} = ABD_{opt}\left[\left(1 - \frac{A_b}{2A_f}\right)^2 - 1\right]}$$

The border area was obtained in Fiji by first thresholding the corrected optical image output in the homogeneity data set (Section 5), at the same threshold as the original analysis. The pencil tool was used to separate any inner features from the border, as seen in the left pane of Figure 7. This stack was then duplicated and the particle images filled in the duplicated stack. The area was then

determined for the two stacks using the Analyze Particles feature in Fiji. We performed this analysis on 23 to 24 particles for each particle size from the homogeneity measurement data set, with results given in Table 6.

Table 6. Values of the actual ABD minus apparent ABD, for the optical border model.

	100 µm ABD	**150 µm ABD**	**220 µm ABD**
		Actual - Apparent, µm	
	ABD Corr	ABD Corr	ABD Corr
	-2.83	-2.84	-3.50
	-2.84	-2.86	-3.45
	-2.85	-2.89	-3.32
	-2.74	-2.54	-3.38
	-2.75	-2.52	-3.39
	-2.71	-2.55	-2.70
	-2.62	-2.58	-2.74
	-2.71	-2.60	-2.62
	-2.50	-2.56	-2.82
	-2.86	-2.93	-2.90
	-2.69	-2.94	-2.97
	-2.71	-2.93	-2.68
	-2.56	-3.20	-2.77
	-2.57	-3.21	-2.71
	-2.61	-3.22	
Average	-2.70	-2.82	-3.00
ESDM	0.03	0.07	0.09

Model 2: Optical 1/NA Extrapolation Model

Optical resolution theoretically scales as 1/NA, where NA is the numerical aperture of the objective. For measurements at high magnification, we would like the particles to be as flat as possible and immobilized, so we are sure to always measure the same particle. To achieve this, we lightly glued down five particles of each size onto a glass microscope slide and then imaged each particle at a different numerical aperture (10 × (0.3 NA), 20 × (0.45 NA), and 40 × (0.55 NA).

Thresholding setting, which would give 50 % completion of a full border, and analysis proceeded according to the regular procedure used for the apparent size measurements (Section 4.2.1). Inspection of the stage micrometer calibration results showed that 40 × images had noticeable pincushion distortion. Images can be transformed to eliminate pincushion distortion, but this method is laborious. A comparison of the untransformed and transformed results showed less than 0.15 % variation in ABD, so on this basis, the analysis continued without a correction for pincushion effects.

Plotting the measured size versus 1/NA, the *y* intercept is an estimate of the size at infinite resolution. Lack of particle flatness, non-vertical sidewalls, or second-order effects in the dependence of diffraction on particle thickness may cause deviations from this simple linear behavior. This, too, is a Type B uncertainty that is hard to quantify. We expect that these effects are more likely to increase the apparent border thickness at large NA (high magnification) than at small NA, and if this is so, the intercept will be somewhat larger than the actual size. For this reason, this method gives a likely lower limit on the correction magnitude, within the repeatability of the measurements.

The particles measured for this model were independent of those measured for the optical border model. Extrapolation plots are shown in Figure 8. We are only interested in determining the slope of the ABD or MFD versus 1/NA from the five measured particles, and not the actual ABD or MFD. Once the average slope is found, the correction actual size minus apparent optical size is equal to the negative of the average slope times 1/NA for the 10 × objective. The same analysis can be done for the MFD. The Feret analysis is potentially noisier, since the ABD measurement effectively averages over all portions of the perimeter, whereas the MFD depends on the location of two extremities of the particle. In addition to the absence of statistical averaging of multiple particle locations, the extremities may also be more susceptible to lifting off the slide surface. Table 7 gives a summary of the results, with all slopes in units of micrometers.

Correction values to add to the measured ABD and MFD are obtained by multiplying the negative of the average slope by the 1/NA value of the 10 × objective. These correction values are listed under ABD correction or MFD correction in Table 7.

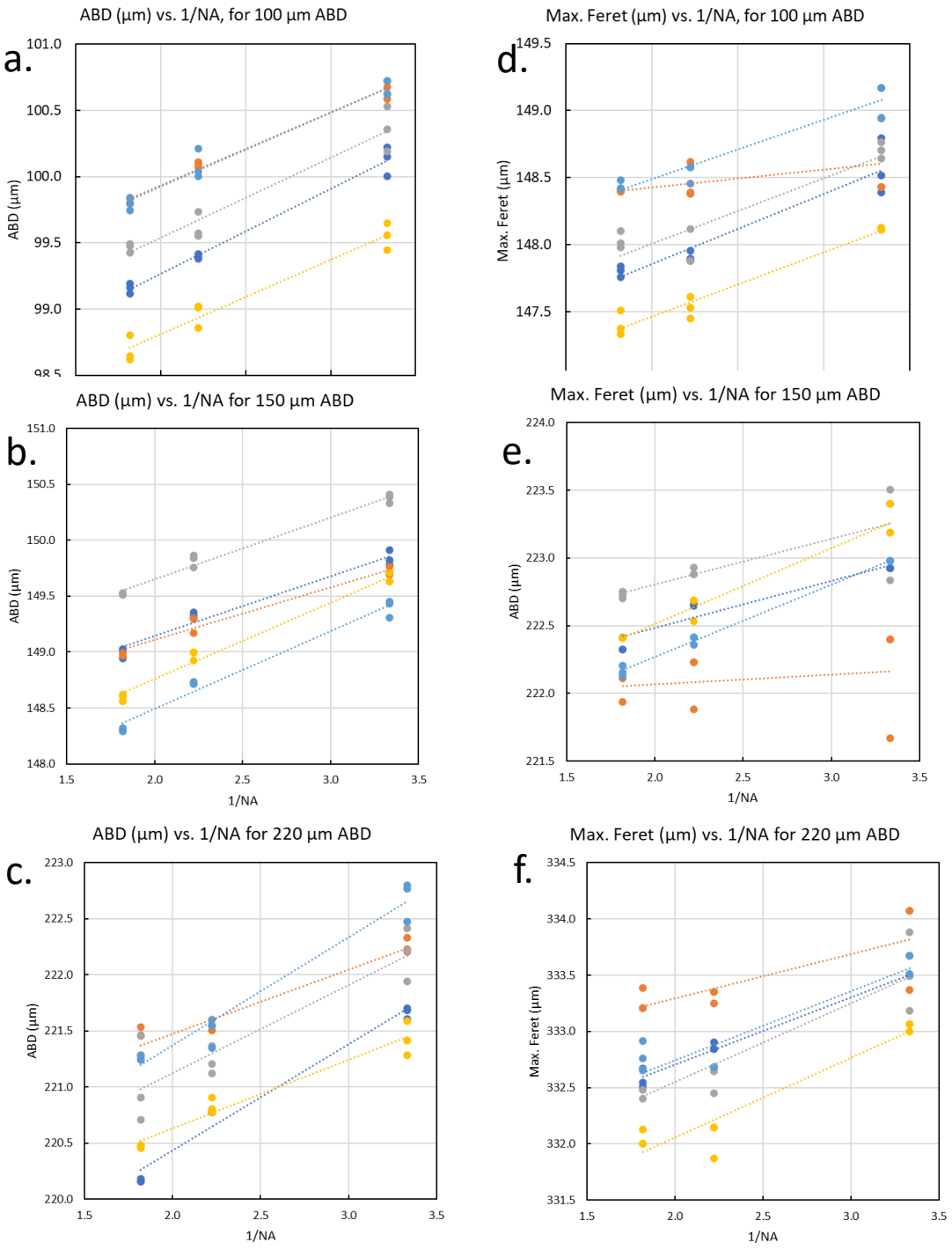

Figure 8. Plots of apparent ABD and MFD versus 1/NA for five particles of each size. Different colors correspond to different individual particles.

Table 7. Slope and correction values for apparent ABD and MFD versus 1/NA, for three particle sizes. All values have units that are in micrometers.

100 µm ABD

Particle	Slope (ABD vs. 1/NA)	ABD Correction	Slope (MFD vs. 1/NA)	MFD Correction
1	0.643	−2.143	0.523	−1.743
2	0.553	−1.843	0.132	−0.440
3	0.606	−2.020	0.491	−1.637
4	0.561	−1.870	0.480	−1.600
5	0.558	−1.860	0.445	−1.483
Avg. Slope	0.584	−1.947	0.414	−1.381
SD	0.039	0.130	0.160	0.534
ESDM	0.018	0.058	0.072	0.239

150 µm ABD

Particle	Slope (ABD vs. 1/NA)	ABD Correction	Slope (MFD vs. 1/NA)	MFD Correction
1	0.535	−1.783	0.349	−1.163
2	0.469	−1.563	0.071	−0.237
3	0.553	−1.843	0.338	−1.127
4	0.684	−2.280	0.56	−1.867
5	0.696	−2.320	0.534	−1.780
Avg. Slope	0.587	−1.958	0.370	−1.235
SD	0.099	0.329	0.196	0.654
ESDM	0.044	0.147	0.088	0.292

220 µm ABD

Particle	Slope (ABD vs. 1/NA)	ABD Correction	Slope (MFD vs. 1/NA)	MFD Correction
1	0.949	−3.163	0.599	−1.997
2	0.570	−1.900	0.394	−1.313
3	0.789	−2.630	0.702	−2.340
4	0.612	−2.040	0.708	−2.360
5	0.963	−3.210	0.616	−2.053
Avg. Slope	0.776	−2.589	0.604	−2.013
SD	0.183	0.611	0.127	0.424
ESDM	0.082	0.273	0.057	0.190

Model 3: SEM – Optical Area

In theory, the most straightforward approach to determine the size difference between optically measured particles and the actual size is to measure the same particles both optically and with high-resolution electron microscopy. Scanning Electron Microscopy gives a spatial resolution that is significantly better than optical microscopy, and the edges have no discernible diffraction effects.

Electron microscopy images showed very good edge definition, but the contrast was variable for different parts of the border. To obtain good separation of particles from the background, we preprocessed the images by performing a Fast Fourier Transform bandwidth filtration in Fiji, choosing a bandwidth between (1 and 15) pixels. Following this transformation, the particles were segmented by manually choosing a threshold that was as low as possible while keeping the number of "false positive" pixels low enough to avoid any noticeable distortion of the particle edges.

Consequently, we can take the edge of the SEM particle image as representative of the actual particle edge. Optical analysis was done similarly as was described in the apparent size section, by setting the threshold to be halfway between the background intensity and the intensity corresponding to the dark portion of the border. Analysis of both sets of images gave ABDs. The difference in ABD between optical and SEM images is taken as the difference between the apparent optical diameters and the presumed actual (i.e., SEM) diameter. Because we performed optical and electron microscopy in a paired manner on specific particles, random variations in particle size do not affect the measurement.

In practice, though, we found that the electron microscopy results were more variable than anticipated and sometimes gave differences from the optical results larger than the "upper-limit" Model 1. Closer analysis revealed that the electron microscopy images were sometimes distorted. This problem was more pronounced for the 220 μm ABD particles than the smaller particles, and the effects were variable from particle to particle, suggesting the problem was likely from beam-charging effects of the uncoated polymer particles. To circumvent this problem, we note that the distances from hole to hole can be determined from the optical images independent of diffraction effects (and thus very accurately), since increased diffraction does not alter the perceived position of the center of a hole. We measured the distances between sets of holes; we will refer to these distances as "chords". The electron microscopy image results were then scaled by the ratio of observed chord lengths. In effect, the particles have their own internal rulers used to calibrate the images.

Figure 9 illustrates the chords measured for the three sizes of particles. For 100 μm and 150 μm ABD particles, the chord lengths were close to that expected, and we selected two chords that were approximately perpendicular. For the 220 μm ABD particles, the distortion was larger, and we were not sure if the long "limb" on the particle was representative of the bulk of the particle, so we chose one chord on the long dimension of the particle and two chords across the shorter dimension of the particle.

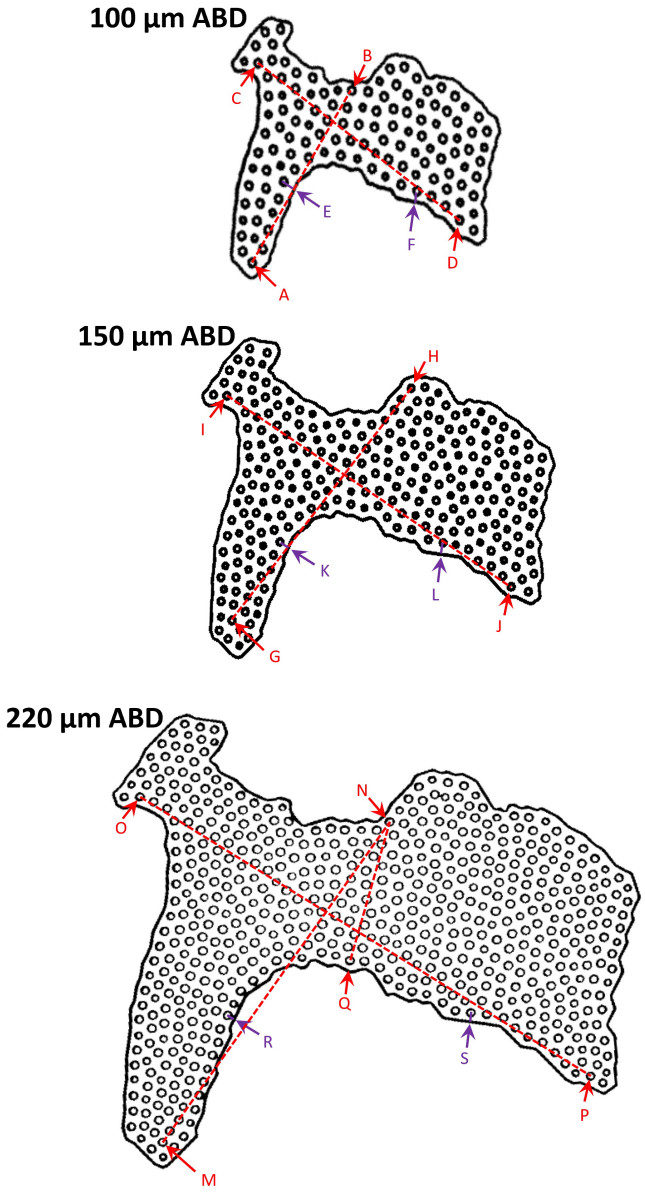

Figure 9. Schematics of the three particle sizes indicating measured chord and hole-to-edge locations. The red letters and lines are used to represent the different chords as described in Model 3. The purple letters and arrows represent the hole-to-edge lengths used in Model 4.

Corrected SEM values were obtained from the following equations:

[2] $$\mathbf{ABD_{corr,SEM}} = \boldsymbol{C_{ABD}} \cdot \mathbf{ABD_{SEM}}$$

[3] $$\mathbf{MFD_{corr,SEM}} = \boldsymbol{C_F} \cdot \mathbf{MFD_{SEM}}$$

where ABD_{SEM} and MFD_{SEM} are the original ABD and MFD from the SEM image analysis, and C_{ABD} and C_F are scaling factors obtained from the measured ratios R of the optically determined chord length to that determined on the SEM image. The ratio for ABD is the geometric average of the chord ratios in two orthogonal directions; the ratio for the MFD is the ratio for the chord aligned with the MFD axis:

[4] 100 µm ABD $$\boldsymbol{C_{ABD}} = \sqrt{\boldsymbol{R_{AB}} \cdot \boldsymbol{R_{CD}}} \qquad \boldsymbol{C_F} = \boldsymbol{R_{CD}}$$

[5] 150 µm ABD $$\boldsymbol{C_{ABD}} = \sqrt{\boldsymbol{R_{GH}} \cdot \boldsymbol{R_{IJ}}} \qquad \boldsymbol{C_F} = \boldsymbol{R_{IJ}}$$

[6] 220 µm ABD $$\boldsymbol{C_{ABD}} = \sqrt{\langle \boldsymbol{R_{NM}}, \boldsymbol{R_{NQ}} \rangle \cdot \boldsymbol{R_{OP}}} \qquad \boldsymbol{C_F} = \boldsymbol{R_{OP}}$$

Table **8** gives values of the chord ratios and resulting scaling and correction factors

Table 8. Values of the chord ratios *R*, scaling factors C_{ABD} and C_F, and corrections $ABD_{corr,SEM} - ABD_{optical}$ and $MFD_{corr,SEM} - MFD_{optical}$ for ABD Corr. and MFD Corr. columns.

100 µm ABD

	Ratio of optical to SEM chord lengths (*R)*		Scaling Factors (C_{ABD} *or* C_F)		Corrections (µm)	
Particle number	Chord CD	Chord AB	ABD factor	MFD factor	ABD Corr.	MFD Corr.
1	1.009	0.998	1.003	1.009	-2.138	-0.836
2	1.002	0.995	0.998	1.002	-1.926	-0.766
3	0.999	1.007	1.003	0.999	-1.535	-1.522
4	1.005	0.997	1.001	1.005	-1.882	-1.243
5	1.003	1.002	1.002	1.003	-2.036	-1.760
Avg.	1.004	1.000	1.001	1.002	-1.903	-1.225
ESDM	0.002	0.002	0.001	0.001	0.102	0.192

150 µm ABD

	Ratio of optical to SEM chord lengths (*R)*		Scaling Factors (C_{ABD} *or* C_F)		Corrections (µm)	
Particle number	Chord IJ	Chord GH	ABD factor	MFD factor	ABD Corr.	MFD Corr.
1	1.014	1.024	1.019	1.014	-2.224	-2.156
2	1.014	1.012	1.013	1.014	-1.172	-0.456
3	1.012	1.012	1.012	1.012	-0.725	-0.973
4	1.007	1.007	1.007	1.007	-1.874	-0.939
5	1.011	0.996	1.004	1.011	-1.806	-0.304
Avg.	1.012	1.010	1.011	1.012	-1.560	-0.966
ESDM	0.001	0.005	0.003	0.001	0.269	0.325

220 µm ABD

	Ratio of optical to SEM chord lengths (*R)*			Scaling Factors (C_{ABD} *or* C_F)		Corrections (µm)	
Particle number	Chord NM	Chord OP	Chord NQ	ABD factor	MFD factor	ABD Corr.	MFD Corr.
1	1.016	1.008	1.018	1.012	1.008	-1.891	-1.974
2	1.017	1.015	1.031	1.019	1.015	-3.420	-0.789
3	1.055	1.016	1.049	1.034	1.016	-1.765	-0.996
4	1.031	1.02	1.03	1.025	1.02	-1.879	-0.664
5	1.088	1.013	1.056	1.042	1.013	-1.177	-1.060
Avg.	1.041	1.014	1.037	1.026	1.014	-2.026	-1.097
ESDM	0.014	0.002	0.007	0.005	0.002	0.372	0.231

Model 4: SEM − Optical Border

An alternate analysis of the SEM and optical images that is much less sensitive to image distortion is to compare the distance between the particle edge and adjacent holes for the two methods. For each of the three particle sizes, we measured the distance between the center of holes and the particle edge for two locations on five particles. The locations were chosen to be sections of the outer perimeter that were straight, so that it was easy by eye to draw a chord from the center of one of the circular holes to the particle edge, keeping the chord normal to the edge, as shown in Figure 10). This measurement is manual but straightforward. Distances were all determined as the distance from the hole to the middle of the border since this is easy to determine visually. To obtain the desired correction referenced to the outer edge of the optical image, we need to add the correction from the Optical Border Model (Model 1) to the SEM − Optical Border Model (Model 4). The Type A uncertainties of the final correction are, therefore, the combinations of the Type A uncertainties of the two models. Table 9 summarizes these calculations and values. The map # refers to the particle number supplied for the SEM measurements, and the positions refer to the purple letter codes seen in Figure 9.

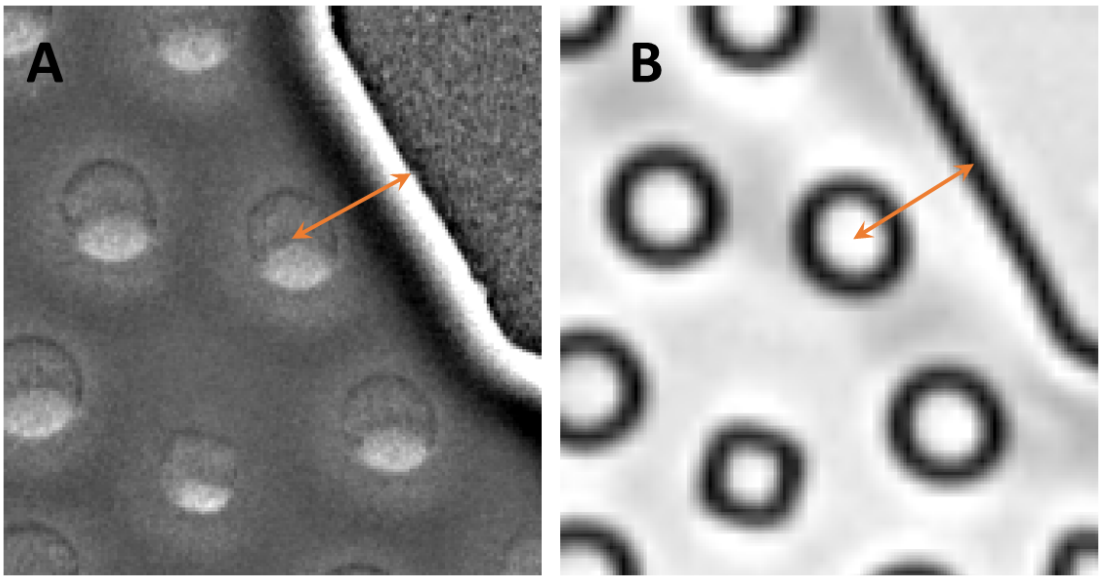

Figure 10. Close-up images of the particles (A) SEM image with orange line indicating hole-to-edge distance; (B) optical image with orange line indicating hole to edge distance, with the edge chosen as defined by the optical border model.

Table 9. Corrections for actual minus apparent ABD for three particle sizes. The top portion of the table shows corrections relative to the edge as defined by the optical border model; the lower portion of the table adjusts these values to give the actual ABD minus the apparent optical ABD. The positions (indicated by purple letters and arrows) are shown in Figure 9.

	100 µm ABD			150 µm ABD			220 µm ABD	
ABD corrections, Actual – Optical border model (µm)								
	SEM – Optical border diam. basis, µm			SEM – Optical border diam. basis, µm			SEM – Optical border diam. basis, µm	
Map #	Pos. E	Pos. F	Map #	Pos. K	Pos. L	Map #	Pos. R	Pos. S
1	0.56	0.02	1	0.03	0.12	1	2.99	3.24
2	-1.19	-1.05	2	0.59	-0.33	2	1.36	-1.28
3	-0.03	1.65	3	-0.92	-1.97	3	2.52	-3.56
4	-0.27	-0.91	4	0.24	1.76	4	-0.13	1.55
5	-0.44	0.99	5	0.93	0.47	5	-1.92	1.36
Ave	-0.27	0.14	Ave	0.17	0.01	Ave	0.97	0.26
ESDM	0.28	0.53	ESDM	0.31	0.6	ESDM	0.9	1.2
Average of both positions								
Actual – Optical border	Ave.	-0.07		Ave.	0.09		Ave.	0.61
	ESDM	0.29		ESDM	0.32		ESDM	0.72
Optical border – Apparent 10x ABD	Ave.	-2.70		Ave.	-2.82		Ave.	-3.00
	ESDM	0.03		ESDM	0.07		ESDM	0.09
Actual – Apparent ABD	Ave.	-2.77		Ave.	-2.73		Ave.	-2.38
	ESDM	0.29		ESDM	0.33		ESDM	0.72

Summary of the actual vs. measured models

The four models agree quite well, as summarized in Table 10. The optical "upper limit" and "lower limit" models are correctly ordered for all three particle sizes. The SEM determinations are consistent with the optical determinations. Looking at the data, the variation across particle size is minimal, and it may be reasonable to use a single pooled value for ABD (SEM) – ABD (optical).

Two of the models can also be applied to the analysis of the MFD, and we have done that as well. The MFD corresponds to measurements from one tip to another tip of the particles. Theoretically, if we assume that diffraction causes a uniform dilation of the particle by the distance δ, the MFD will increase by 2δ. In contrast, the increased convolution of the particles compared to a circle gives a larger fractional change in the ABD. This change in ABD is given as

$$[7] \qquad \mathbf{\Delta ABD} = \frac{\mathbf{2}C\boldsymbol{\delta}}{\mathbf{1}+{}^{\mathbf{\Delta ABD}}/_{\mathbf{2ABD}}} \approx \mathbf{2}C\boldsymbol{\delta},$$

where C = 1.70 is the ratio of the visible particle perimeter to the perimeter of an equivalent circle. Thus, the ratio of the MFD correction to the ABD correction is theoretically expected to be $1/C$ = 0.59 for the present particles. Given that there are only two models for the MFD correction, the use of this relation may be a better alternative than only using the two models directly.

Table 10. Summary of actual minus apparent ABD and MFD corrections , for the four models.

100 ABD

ABD(µm), correction to be applied to 10× optical to obtain actual

Model	Optical Border	Optical 1/NA extrapolation	SEM - Optical, Area	SEM - Optical, Border
Ave. corr.	-2.70	-1.95	-1.90	-2.77
u , Type A	0.03	0.06	0.10	0.29

MFD(µm), correction to be applied to 10× optical to obtain actual

Model		Optical 1/NA extrapolation	SEM - Optical, Area	
Ave. corr.	NA	-1.38	-1.23	NA
u , Type A		0.24	0.19	

150 ABD

ABD(µm), correction to be applied to 10× optical to obtain actual

Model	Optical Border	Optical 1/NA extrapolation	SEM - Optical, Area	SEM - Optical, Border
Ave. corr.	-2.82	-1.96	-1.56	-2.73
u , Type A	0.07	0.15	0.27	0.33

MFD(µm), correction to be applied to 10× optical to obtain actual

Model		Optical 1/NA extrapolation	SEM - Optical, Area	
Ave. corr.	NA	-1.23	-0.97	NA
u , Type A		0.29	0.33	

220 ABD

ABD(µm), correction to be applied to 10× optical to obtain actual

Model	Optical Border	Optical 1/NA extrapolation	SEM - Optical, Area	SEM - Optical, Border
Ave. corr.	-3.00	-2.59	-2.03	-2.38
u , Type A	0.09	0.27	0.37	0.72

MFD(µm), correction to be applied to 10× optical to obtain actual

Model		Optical 1/NA extrapolation	SEM - Optical, Area	
Ave. corr.	NA	-2.01	-1.1	NA
u , Type A		0.19	0.23	

4.2.3. Comparison of ABD and MFD between different microscopes

The optical images obtained during this study can also be compared to the images obtained on Microscope 1 with the Palmer Chamber and Microscope 2. Optical images for particles on gold-coated slides were obtained before and after imaging in the SEM, to ascertain if there were any changes in particle size. Using a paired *t*-test, no statistically significant ($p < 0.05$) changes were seen between optical sizes obtained before and after SEM exposure.

However, we were quite surprised to see that the particles mounted on gold-coated slides have visually sharper edges than the particles contained in a glass Palmer Chamber, even when imaged with identical microscopes (see Figure 11). With sharper borders, we surmised that the apparent optical size of the particles on gold-coated slides would be smaller than the sizes when mounted in the Palmer Chamber. Because we had only five particles of each size, we scaled the measured ABD and MFD by the ratio of the lengths of the internal hole-to-hole chords for the set of particles characterized by Microscope 1 for size and homogeneity to that of the five measured particles. In effect, we are matching internal dimensions of the different particle lots and then seeing what difference remains for the external dimensions. Note that unlike the analysis of the SEM images, there was no evidence of image distortion—we are uniformly scaling the particle size of the lot of five particles to match the mean particle size as measured for many particles in the Palmer Chamber on Microscope 1. The chord-scaling process gave the scaling factors for the particles on gold listed in Table 11.

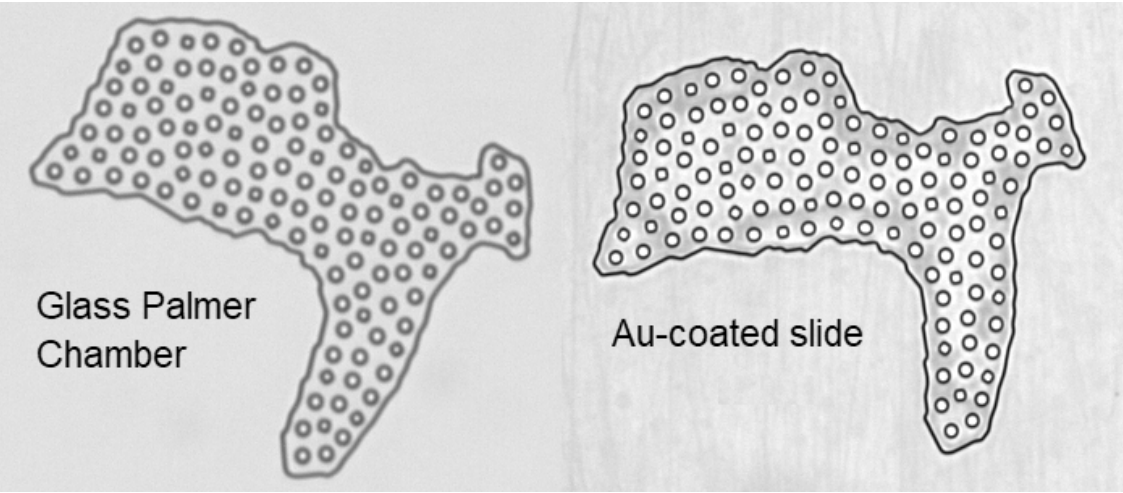

Figure 11. Microscopic images of particles contained in a Palmer Chamber (left) versus on a gold-coated slide (right), with all other optical parameters fixed except for the intensity of incident light. Both particles were immersed in water.

Table 11. Scaling factor to adjust the gold-mounted particles to match the internal dimensions measured for the main lot of measured particles.

	Scaling factor Main Lot/Au Lot
100 µm ABD	1.003
150 µm ABD	0.994
220 µm ABD	0.998

Optical results of the particles on gold are given in Table 5 and Table 12. As seen in Table **3**, Table 4, and Table 5, we find that the particles measured by Microscope 2 are intermediate in size relative to the two results obtained on Microscope 1 for particles in the Palmer Chamber and particles adhered to a gold-coated slide. Thus, we can see that differences in particle mounting can lead to differences in optical image size, even if the operator, microscope, camera, and settings are otherwise fixed.

Table 12. Results for the apparent optical ABD and MFD , after correction by the scaling factors in Table 11, for data obtained before and after measurement by SEM.

Average apparent optical sizes, prior & post SEM

100 µm ABD

	ABD	MFD	Min. Feret
# particles	5	5	5
Ave., µm	98.98	148.25	112.90
SD, µm	0.38	0.40	0.34
RSD	0.38%	0.27%	0.30%
ESDM, µm	0.17	0.18	0.15

150 µm ABD

	ABD	MFD	Min. Feret
# particles	5	5	5
Ave., µm	148.13	222.19	168.99
SD, µm	0.71	0.83	0.61
RSD	0.48%	0.38%	0.36%
ESDM, µm	0.32	0.37	0.27

220 µm ABD

	ABD	MFD	Min. Feret
# particles	5	5	5
Ave., µm	221.81	333.45	253.70
SD, µm	1.39	2.27	1.72
RSD	0.63%	0.68%	0.68%
ESDM, µm	0.62	1.02	0.77

5. Homogeneity of SRM 1989

For homogeneity assessment of the size, 10 vials were removed from each of the 3 size ranges for data collection and analyzed on Microscope # 1 using a Palmer Chamber. The 10 vials were selected using a stratified sampling plan; the lots were separated into sequential sub-lots of 20 vials and 1 vial was randomly selected from each sub-lot. The vials were numbered before the fill, so the numbers represent the order of the vials during filling, i.e., lower vial number vials were filled earlier than the higher vial number vials.

The homogeneity of the particle number concentration was also evaluated as it was important to know that the particle number concentrations in the vials were uniform throughout the fill.

5.1. Size

The measurements of the particle size were performed, and data were analyzed as described in the apparent size section. The data were collected by 2 analysts on separate days; this resulted in 2 separate data sets for each vial. Each analyst manually refocused the camera for each particle. For each size range, at least 8 particle images were collected per vial. One vial from each size was also analyzed on Microscope #2 for information on instrumental variability.

The three sizes of SRM 1989 display excellent homogeneity. The small standard deviation of the size, in Table 13, indicate a tight distribution around the size range of interest. This was expected since homogeneity was initially assessed during the release and production of the particles from the wafers, as was described in Section 3 Production of SRM 1989 .

Table 13. Sizing data of the 3 particle sizes of SRM 1989, acquired by two analysts, showing both within vial variability and between vial variability. SD represents standard deviation; the average ABD ± 1 SD and MFD and ± 1 SD is shown.

Vials	Analyst 1				Analyst 2			
100 µm								
Vial Number	**ABD (µm)**	**ABD SD (µm)**	**MFD (µm)**	**MFD SD (µm)**	**ABD (µm)**	**ABD SD (µm)**	**MFD (µm)**	**MFD SD (µm)**
80	100.89	0.39	149.35	0.22	100.85	0.38	149.20	0.17
146	100.63	0.27	149.19	0.32	100.56	0.46	148.95	0.66
190	100.73	0.58	149.27	0.43	100.56	0.39	149.08	0.31
11	100.66	0.46	149.07	0.43	100.61	0.62	149.14	0.35
28	100.73	0.62	149.26	0.39	100.44	0.66	148.99	0.69
53	100.68	0.30	149.26	0.31	100.87	0.54	149.19	0.46
87	100.65	0.36	149.13	0.32	100.31	0.49	148.55	0.54
112	100.67	0.39	149.05	0.67	100.53	0.38	149.09	0.39
176	100.69	0.61	149.24	0.48	100.65	0.56	149.08	0.46
Average, µm	**100.70**		**149.20**		**100.60**		**149.03**	
SD, µm	**0.08**		**0.10**		**0.18**		**0.20**	
RSD (%)	**0.08**		**0.07**		**0.18**		**0.13**	
150 µm								
Vial Number	**ABD (µm)**	**ABD SD (µm)**	**MFD (µm)**	**MFD SD (µm)**	**ABD (µm)**	**ABD SD (µm)**	**MFD (µm)**	**MFD SD (µm)**
61	150.13	0.54	222.84	0.84	150.56	0.57	223.32	0.59
92	150.50	0.54	223.37	0.57	150.33	0.51	223.16	0.49
136	150.58	0.38	223.57	0.35	149.67	0.23	222.72	0.34
146	150.16	0.64	222.97	0.66	150.13	0.54	223.06	0.54
9	150.20	0.50	223.12	0.37	150.14	0.49	223.04	0.42
38	150.02	0.49	223.23	0.32	150.11	0.66	223.23	0.61
52	150.31	0.55	223.15	0.51	149.92	0.45	222.84	0.52
109	150.10	0.53	223.03	0.55	150.06	0.57	223.02	0.52
175	149.91	0.50	222.78	0.52	150.15	0.41	223.08	0.45
189	150.12	0.57	223.04	0.66	150.13	0.43	223.12	0.33
Average, µm	**150.20**		**223.11**		**150.12**		**223.06**	
SD, µm	**0.21**		**0.24**		**0.23**		**0.18**	
RSD (%)	**0.14**		**0.11**		**0.16**		**0.08**	
220 µm								
Vial Number	**ABD (µm)**	**ABD SD (µm)**	**MFD (µm)**	**MFD SD (µm)**	**ABD (µm)**	**ABD SD (µm)**	**MFD (µm)**	**MFD SD (µm)**
6	222.47	0.36	333.45	0.52	222.19	0.15	333.19	0.40
33	222.47	0.41	333.33	0.77	222.28	0.32	333.14	0.73
59	222.60	0.57	333.45	0.44	222.17	0.41	333.05	0.53
66	222.26	0.86	333.22	0.59	222.32	0.20	333.13	0.58
83	222.47	0.26	333.48	0.52	222.72	0.46	333.72	0.51
109	222.30	0.34	333.32	0.27	222.45	0.18	333.32	0.44
132	222.56	0.25	333.61	0.24	222.23	0.46	333.09	0.56
156	222.46	0.14	333.53	0.25	222.23	0.30	333.34	0.61
174	222.31	0.22	333.43	0.43	222.39	0.65	333.07	1.13
183	222.48	0.45	333.34	0.64	222.41	0.28	333.61	0.39
Average, µm	**222.44**		**333.42**		**222.34**		**333.27**	
SD, µm	**0.11**		**0.11**		**0.16**		**0.23**	
RSD (%)	**0.05**		**0.03**		**0.07**		**0.07**	

For quantifying the amount of variability between vials, we fit a linear mixed effect model estimated using restricted maximum likelihood implemented via the "lme4" R package (12). Treating vial number as a random effect and size as a categorical, fixed effect, the model estimates the variability due to vial number to be zero for all sizes for ABD and MFD. The data from each vial across size groups is shown in Figure 12 below. While there is naturally some variability between vials, this amount is negligible compared to the variability at the replicate level.

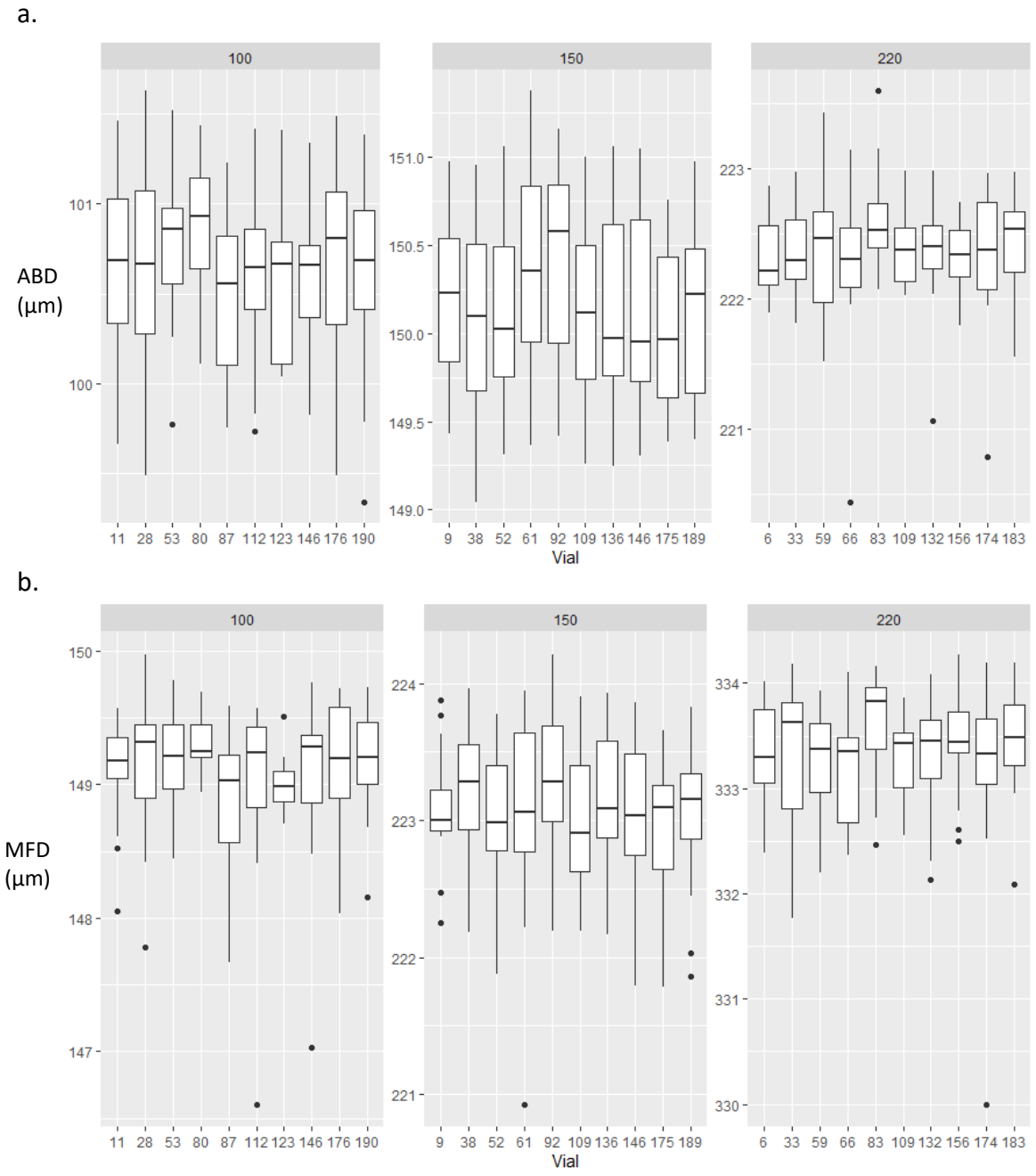

Figure 12. Size distribution for different vials of SRM 1989 at the 3 sizes for a) ABD and b) MFD.

5.2. Particle Number Concentration

The three size ranges of SRM 1989 display acceptable homogeneity regarding the number concentration of the particles for its intended use. It is important to reiterate here that this standard is primarily a size standard; a concentration is useful primarily so that the analyst can make the appropriate dilutions. Vial variability is the largest estimated source of number concentration variability, as described in Appendix A. Moreover, the largest vial variability is only roughly 7 % of the mean concentration, which is sufficiently small for most practical purposes.

6. Stability of SRM 1989

Measurements on the apparent size of the particles were carried out 9 months (t = 9 months) after the initial sample preparation and measurement. The same vials used for homogeneity testing were imaged by one analyst using only the Kiralux camera on Microscope #1. In this case the homogeneity measurements are defined as the time = 0 months measurements. For the stability measurement, fewer particles from fewer vials were imaged compared to the homogeneity measurements. All the images were processed in a nearly identical manner for the homogeneity and stability measurements, as was described earlier.

Tables 14 and Table 15 provide summary information on the changes in particle size over 9 months for the ABD and MFD measurements, respectively. There are no statistically significant differences in both ABD and MFD in the 3 particle sizes over this time frame indicating robust size stability of SRM 1989.

The first column indicates the size group, and the 2nd through 5th columns provide the mean and standard deviations of the observations at the starting time point and 9 months later. The change in size, ESDM (experimental standard deviation of the mean), and the p-values are shown in columns 6, 7, and 8 of Table 14 and Table 15. The change in size was obtained by simply subtracting the average sizes at t = 9 months from t = 0 months. The change is negative if the size has decreased relative to the measurement at t = 0 months and is positive if the size has increased relative to the measurement taken at t = 0 months. The ESDM and p-value were computed using a 2-sample t-test with pooled variances. Although the difference for the 100 µm MFD group is almost statistically significant at an $\alpha = 0.05$ type I error rate, the differences are small with respect to the total variability in the uncertainty budget.

Table 14. Stability results for apparent ABD over 9 months for the 3 particle sizes. Time (*t*) units are all in months.

Nominal Particle Size (µm)	ABD (*t* = 0) (µm)	ABD (*t* = 0) SD (µm)	ABD (*t* = 9) (µm)	ABD (*t* = 9) SD (µm)	Change in size (µm)	ESDM (µm)	p-value
100	100.65	0.47	100.61	0.46	-0.04	0.08	0.61
150	150.16	0.53	150.01	0.56	-0.15	0.10	0.12
220	222.39	0.41	222.42	0.39	0.03	0.07	0.66

Table 15. Stability results for apparent MFD over *t* = 9 months for the 3 particle sizes. Time (*t*) units are all in months.

Nominal Particle Size (µm)	MFD (*t* = 0) (µm)	MFD (*t* = 0) SD (µm)	MFD (*t* = 9) (µm)	MFD (*t* = 9) SD (µm)	Change in size (µm)	ESDM (µm)	p-value
100	149.11	0.46	149.24	0.39	0.13	0.07	0.06
150	223.08	0.53	223.08	0.53	0.00	0.09	1.00
220	333.33	0.58	333.30	0.57	-0.03	0.10	0.76

7. Statistical Evaluation of Data

For each of the three particle sizes, (100, 150, and 220) µm, we provide the certified value for the apparent and actual particle size in terms of the Area Based Diameter (ABD) and Maximum Feret Diameter (MFD) as well as uncertainty values representing the contributions of various sources of errors to these values.

7.1.1. Size Analysis

The statistical model for a measurement of particle size Y, for both ABD and MFD, is assumed to be as follows:

$$[8] \qquad \boldsymbol{Y = \mu + \sum_j \epsilon_j} \quad \text{for } \boldsymbol{j = 1, \ldots, 5}.$$

Above, μ is the unknown measurand to be estimated, and the ϵ_j represent sources of random deviation for measurements of particle size owing to the 5 factors of variability due to analyst, the instrument, optical setup, stability of the sample, and experimental error. The sources of uncertainty are assumed to be independent with finite variance such that

$$[9] \qquad \text{Var}(\boldsymbol{Y}) = \boldsymbol{\sum_j \sigma_j^2} \quad \text{for } \boldsymbol{j = 1, \ldots, 5}.$$

where we define $\text{Var}\left(\epsilon_j\right) := \sigma_j^2$. We then estimate the standard uncertainty for Y as:

$$[10] \qquad \boldsymbol{u(Y) = \sqrt{u(\mu)^2 + \sum_j \sigma_j^2}} \quad \text{for } \boldsymbol{j = 1, \ldots, 5}.$$

All statistical analysis was carried out using the R programming language (13).

7.1.1.1. Uncertainty budget components for apparent size

Apparent size is the diameter (ABD or MFD) inferred from analysis of an optical image; it is not the true size.

The sources of variability for the uncertainty budget, as well as how the values are calculated, are described below in Table 16.

Table 16. Description of the uncertainty budget components for apparent size

Uncertainty Components Definitions
Experimental-This value represents the natural variability inherent to the measurement process under repeated experimental conditions. We calculate this term by computing the standard deviation from the generated data. Specifically, these data consist of 198, 199, and 172 total measurements from the 100 µm, 150 µm, and 220 µm groups, respectively. The standard deviation is an appropriate estimator since there is very little vial-to-vial variability, and the distribution is roughly Gaussian. Furthermore, any deviations from the normality are small compared to the magnitude of the sources of variability. (Type A uncertainty)
Analyst-This term represents the variability due to differences between analysts. To estimate this value, a study was carried out among 5 analysts. Results are pooled among the size groups via taking the root mean square of the standard deviation from each group. Note that we did not include the 220 µm size group in quantifying uncertainty due to analyst, as the variability appeared much smaller than for the other two groups, which may have led to an underestimate of analyst variability. (Type A uncertainty)
Instrument-This value represents the variability due to the difference between the instrument/set-up used. Using the results from 3 different instrumental setups, the DerSimonian-Laird approach was used to estimate the between-instrument variability based on the observed mean, standard deviation, and sample size from the 3 instruments set-ups (14). This was carried out using the "metafor" R package (Type A uncertainty) (15).
Optical Distortion-An additional source of Type B uncertainty, assumed to be 0.1 % of the mean based on inspection of stage micrometer measurements over the camera field of view, was incorporated to account for spatial distortions of camera images (Type B uncertainty).
Stability-Follow-up measurements were taken 9 months after the initial sample preparation and measurements were made. The change in size over 9 months is estimated as the difference in the mean particle size between the sample at the start and the sample at 9 months. For the ABD and MFD, the average of the absolute change over 9 months across all sizes was extrapolated linearly to 5 years, representing a standard uncertainty due to stability (Type A uncertainty).
Estimate-Uncertainty in the mean value of the measurand μ in Equation [8], above. Computed as the experimental standard error of the mean, $s/\sqrt{n}$, where s is the sample standard deviation of the observations used to estimate the mean, and n is the sample size. (Type A uncertainty)

The uncertainty budgets for various factors described above are broken down into individual components and shown below for each of the 3 sizes.

Table 17. Uncertainty budget for apparent size 100 µm; all uncertainties are in units of micrometers.

Source of Uncertainty	ABD Value (µm)	MFD Value (µm)
analyst	0.13	0**
estimate	0.03	0.03
experimental	0.47	0.46
instrument	0.82	0.34
optical distortion	0.10	0.15
stability*	0.49	0.36
total	1.07	0.69

*uncertainty for stability has been extrapolated to 5 years.
**analyst selection of optical focusing of particles contributes negligible uncertainty to MFD.

Table 18. Uncertainty budget for apparent size 150 µm; all uncertainties are in units of micrometers

Source of Uncertainty	ABD Value (µm)	MFD Value (µm)
analyst	0.13	0**
estimate	0.04	0.04
experimental	0.53	0.53
instrument	0.82	0.34
optical distortion	0.15	0.22
stability*	0.49	0.36
total	1.11	0.76

*uncertainty for stability has been extrapolated to 5 years.
** analyst selection of optical focusing of particles contributes negligible uncertainty to MFD.

Table 19. Uncertainty budget for apparent size 220 µm; all uncertainties are in units of micrometers.

Source of Uncertainty	ABD Value (µm)	MFD Value (µm)
analyst	0.13	0**
estimate	0.03	0.04
experimental	0.41	0.58
instrument	0.82	0.34
optical distortion	0.22	0.33
stability*	0.49	0.36
total	1.07	0.83

*uncertainty for stability has been extrapolated to 5 years.
**analyst selection of optical focusing of particles contributes negligible uncertainty to MFD.

The apparent size results are summarized in the tables below. Values in column 2 for Table **20** and Table 21 are the Apparent ABD or Apparent MFD obtained from Microscope 1.

The third column, or standard uncertainty (u(ABD) or u(MFD)), was obtained by combining the individual contributions to the uncertainty budget via the root sum of squares. The expanded uncertainty (U(ABD) or U(MFD)) is obtained by multiplying the standard uncertainty u by the coverage factor, set to $k = 2$.

Table 20. Apparent ABD size and expanded uncertainty (k = 2) for the 3 size ranges (u(ABD) representing standard uncertainty and U(ABD) representing the expanded uncertainty).

Nominal Particle Size (µm)	Apparent ABD (µm)	u(ABD) (µm)	U(ABD) (µm)	k
100	100.65	1.07	2.15	2
150	150.16	1.11	2.21	2
220	222.39	1.07	2.14	2

Table 21. Apparent MFD size and expanded uncertainty (k = 2) for the 3 size ranges (u(MFD) representing standard uncertainty and U(MFD) representing the expanded uncertainty).

Nominal Particle Size (µm)	Apparent MFD (µm)	u(MFD) (µm)	U(MFD) (µm)	k
100	149.11	0.69	1.37	2
150	223.08	0.76	1.51	2
220	333.33	0.83	1.66	2

7.1.1.2. Apparent versus Actual Size

In this section so far, we have primarily looked at the apparent size data. Actual size, on the other hand, is the true size of the particle. While the actual size was not directly measured, several experiments were carried out to explore the difference between the apparent and actual particle size, such that the systematic biases that are a natural feature of the apparent measurements are minimized. Specifically, four different methods, detailed in the section 4.2.2 were performed as different ways of measuring the bias from the apparent particle size measurements. To combine the results from these four different methods into a correction estimate, as well as to characterize the uncertainty of that estimate, we used the "rma" function from the "metafor" R package which is used for meta-analyses and consensus estimation. For this analysis, we specifically used the DerSimonian-Laird procedure to combine the results from the four different methods. For this approach, each method is treated as an independent estimate of the true correction factor, and their four estimates (and their individual uncertainties) are combined into a consensus estimate of the correction factor. This procedure notably takes into account both within and between-method variability in its consensus estimate and associated variability. A summary of the definitions and how the corrections are calculated are given in Table 22. The uncertainty contributions to apparent and actual size are shown in Table 23 and Table 24.

Table 22. Apparent and actual sizes and their corrections

Definitions
Apparent: The mean from the observed (apparent) data. These data are from Microscope 1.
***u*(Apparent)**: The uncertainty (standard error) associated with the observed (apparent) mean
***U*(Apparent):** The expanded uncertainty with *k = 2,* associated with the observed (apparent) mean.
Correction: The correction, based on 4 methods of estimating the difference between actual size value and apparent size measurements.
***u*(Correction)**: The uncertainty of the correction between actual and apparent measurements. Four different methods were carried out to provide a single estimate of the difference between apparent and actual measurements. Since there is naturally variability between different methods, we incorporate this into our uncertainty budget. Specifically, we use a linear mixed model fit via restricted maximum likelihood to estimate the uncertainty due to methodology. The "lme4" R package was used to carry out this analysis (12).
Actual: The actual size, which is computed from adding the correction to the apparent size.
***u*(Actual)**: The uncertainty associated with the actual, computed from combining the uncertainties of the apparent and correction in quadrature.
***U*(Actual):** The expanded uncertainty with *k = 2,* associated with the actual mean.

Table 23. Uncertainty contributions to the apparent and actual ABD sizes for the 3 particle sizes

Nominal Particle Size (μm)	Apparent ABD (μm)	*u*(Apparent) ABD (μm)	*U*(Apparent) ABD (μm)	Correction to ABD (μm)	*u*(Correction) (μm)	Actual ABD (μm)	*u*(Actual) ABD (μm)	*U*(Actual) ABD (μm)
100	100.65	1.07	2.15	-2.27	0.23	98.38	1.10	2.20
150	150.16	1.11	2.21	-2.24	0.31	147.92	1.15	2.30
220	222.39	1.07	2.14	-2.62	0.25	219.76	1.10	2.20

Table 24. Uncertainty contributions to the apparent and actual MFD sizes for the 3 particle sizes

Nominal Particle Size (μm)	Apparent MFD (μm)	*u*(Apparent) MFD (μm)	*U*(Apparent) MFD (μm)	Correction to MFD (μm)	*u*(Correction) (μm)	Actual MFD (μm)	*u*(Actual) MFD (μm)	*U*(Actual) MFD (μm)
100	149.11	0.69	1.37	-1.42	0.12	147.69	0.70	1.40
150	223.08	0.76	1.51	-1.32	0.18	221.76	0.78	1.55
220	333.33	0.83	1.66	-1.66	0.27	331.67	0.87	1.74

The apparent size of the particles includes diffraction effects; therefore, it is always larger than the actual size of the particle.

8. Value Assignment of SRM 1989

8.1.1. Particle size as a certified value

The certified size values (both apparent and actual sizes) for the 3 particle sizes are shown below in Table 25.

Table 25. Certified apparent and actual size, in Area Based Diameter (ABD) and Maximum Feret Diameter (MFD), of the 3 nominally sized particle suspensions that comprise 1 unit of SRM 1989.

Nominal Particle Size (µm)	Apparent ABD (µm) [a]	Actual ABD (µm) [a]	Apparent MFD (µm) [a]	Actual MFD (µm) [a]
100	100.65 ± 2.15	98.38 ± 2.20	149.11 ± 1.37	147.69 ± 1.40
150	150.16 ± 2.21	147.92 ± 2.30	223.08 ± 1.51	221.76 ± 1.55
220	222.39 ± 2.14	219.76 ± 2.20	333.33 ± 1.66	331.67 ± 1.74

[a] Values are expressed as $x \pm U(x)$, where x is the certified value and $U(x)$ is the expanded uncertainty of the certified value, with a coverage factor, $k = 2$. To propagate this uncertainty, treat the certified value as a normally distributed random variable with mean x and standard deviation $U(x)/2$.

8.1.2. Particle number concentration as a value of potential interest

The particle number concentrations values for the 3 particle sizes are shown below in Table 26.

Table 26. Particle number concentration of the 3 particle types as a value of interest for SRM 1989. All sizes are in Area Based Diameter (ABD).

Nominal Particle Size (µm)	Particle conc. (mL^{-1})
100	112
150	99
220	95

9. Recommendations for storage and sample handling of SRM 1989

SRM 1989 vials should be stored at (2 to 8) °C for up to 5 years with minimal change in the size of the particles. It is important to avoid freezing the material or exposing it to elevated temperatures. Brief (1 to 2 days) storage of the vials at room temperature, preferably in the dark, will not be a concern but the samples should be stored in the refrigerator for longer duration.

Upon receiving the vial, users should inspect it to ensure that the vial and cap are in good condition before opening. It is good practice to wipe the vial to remove any extraneous particles before opening, preferably in a particle-free working environment or laminar flow hood.

If the SRM 1989 particles are to be transferred into user vials or containers, it is the user's responsibility to ensure that the vial and cap being used are suitable for this purpose and that they do not shed particles over time.

For optimal consistency, vials should be brought to room temperature after removal from storage (2 to 8) °C. The particles must be resuspended in the solution immediately prior to sample removal. Resuspension can be done by pipette-mixing the solution using a 5 mL pipette. Alternatively, if the sample is capped, the vial may be gently inverted back and forth 10 times. Since these particles are in the 100s of micrometers in size, it is important to use a pipette tip with a large enough opening to allow these particles to pass through unimpeded. It is recommended to use a 1 mL or larger pipette to aliquot these particle solutions. If a smaller pipette tip must be used, it may be necessary to trim the tip to ensure a larger opening; however, note that trimming the tip may result in an inaccurate volume. Aliquots should be withdrawn from the center of the resuspended solution since repeated pipetting from the top or the bottom of the vial may result in shifts in the particle concentration of the suspension due to particle settling. Users may wish to aliquot samples into a different solution and/or vial to make dilute solutions. Care should be taken to use low-particle or particle-free containers. These particles are generally compatible with aqueous solutions of near-neutral pH.

10. Acknowledgements

Research performed in part at the NIST Center for Nanoscale Science and Technology NanoFab.

11. Appendices

Appendix A. Particle Number Concentration

For determining the particle number concentration, three vials were taken from each of the 3 size groups, and 2 to 3 replicate measurements were taken from each of those vials. Furthermore, two observations were then made from each of the replicate measurements, for a total of 4 to 6 observations per vial. The observed raw counts were converted to concentration by dividing each count value by the corresponding mass of the sample and assuming a density of 1 g/mL. The particle number concentration data obtained for each vial are shown below in Figure 13.

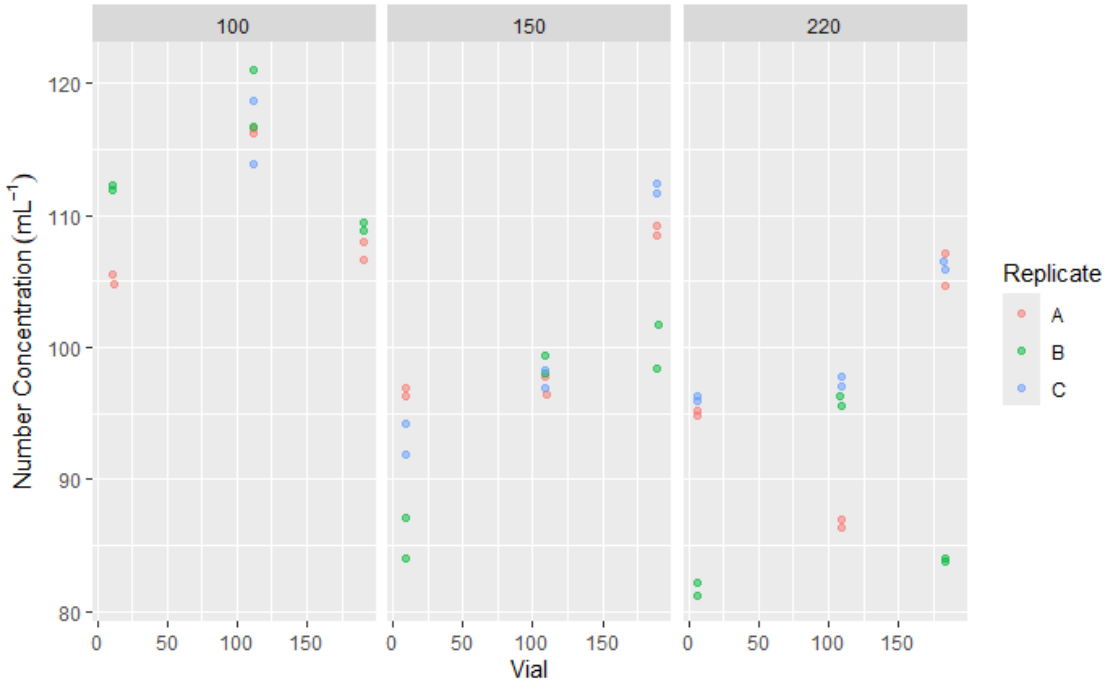

Figure 13. Particle number concentration data for the nominally 100 µm, 150 µm, and 220 µm sized particles. The vial index is on the x-axis, number concentration is on the y-axis, and replicate is indicated by color.

Figure 13 above suggests variability is present at all levels of the experimental structure, as there are differences in the mean between vials, replicates, and repeated measurements (though repeated measurements appear to show the lowest variability). To estimate the amount of variability from each of these 3 sources, we fit a hierarchical Bayesian model assuming Gaussian-distributed random effects at each level of the hierarchy with weakly-informative priors on the mean as well as the variance terms. The parameters for each of the three size groups were calculated independently. Table 27 gives the particle number concentration as well as calculations for each source of uncertainty for the particle number concentrations. The *u*(combined) column below includes all sources of variability we investigated, including the uncertainty of the mean. This value is not calculated via the root sum of squares but by incorporating the full posterior distribution, which takes into account the uncertainty of each variance term. (This results in a larger, more conservative estimate of the combined uncertainty than by using the root sum of squares.) The *u*(vial) represents the variability associated with differences in concentration

between vials due to sample preparation. The *u*(replicate) represents the variability associated with concentration differences between replicate measurements. The *u*(conc.) refers to the uncertainty associated with the concentration measurement process of the same vial and replicate. The *u*(combined) uncertainty represents the combined standard uncertainty for the particle number concentration. The *u*(combined) value thus represents the estimated standard deviation for a typical observation from a similar experimental process.

Table 27. Uncertainty budget for particle number concentration for all 3 sizes

Nominal Particle Size (µm)	Particle number conc. (mL^{-1})	ESDM (mL^{-1})	*u*(vial) (mL^{-1})	*u*(replicate) (mL^{-1})	*u*(conc.) (mL^{-1})	*u*(combined) (mL^{-1})
100	111.59	3.46	4.45	2.79	2.08	7.05
150	98.92	5.38	6.68	5.48	1.51	10.77
220	94.59	4.86	3.91	9.11	0.77	11.66

Appendix B. Particle Morphology

In addition to size, particle morphology data were collected. Maximum Feret Diameter (MFD) is a morphological parameter for irregular shaped particles that is already described throughout this report. Furthermore, parameters such as particle circularity, aspect ratio, and roundness were automatically calculated in Fiji, during data analysis. Circularity and roundness shape descriptors were defined in the following way (16), in accordance with Fiji. The aspect ratio was determined based on the definition used in our previous report on a different reference material (17):

- Circularity: $4\pi \times \frac{[\text{Area}]}{[\text{Perimeter}^2]}$ with a value of 1.0 indicating a perfect circle. As the value approaches 0.0, it indicates an increasingly elongated shape.

- Roundness: $4 \times \frac{[\text{Area}]}{\pi \times [\text{Major Axis}^2]}$.

- Aspect Ratio (AR): The aspect ratio equals the ratio of minimum and maximum Feret diameters, i.e., $\frac{[\text{Min Feret diameter}]}{[\text{Max Feret diameter}]}$. This value will be between 0 and 1.

We strongly caution that the values, especially for roundness and aspect ratio, can vary substantially based on the definition used (18). The values obtained for the above 3 shape parameters are shown in Table 28 and Table 29 for the same particles that were acquired and analyzed for the sizing data, i.e. the same data set was used for sizing and for this morphological analysis.

Regardless of the data and microscope used, the circularity of the three particle sizes is approximately 0.36 with virtually no variability, as indicated by a zero-standard deviation. Here the roundness is 0.60, meaning that the shape of the particle is not spherical (generally > 0.9) but also not elongated and fiber-like (closer to 0). The Aspect Ratio (as defined in our previous report) is about 0.76. While these values are not supplied as reference values, knowing the shape parameters for these particles may be useful for some end-users.

Table 28. Size and morphological parameters acquired with Microscope 1

Nominal Particle Size (µm), ABD	**ABD (µm)**	SD (µm)	RSD (%)	**MFD (µm)**	SD (µm)	RSD (%)	**Circularity**	SD	RSD (%)	**AR**	SD	RSD (%)	**Round**	SD	RSD (%)
100	100.65	0.47	0.47	149.11	0.46	0.31	0.36	0.00	1.17	0.76	0.00	0.28	0.60	0.00	0.32
150	150.16	0.53	0.35	223.08	0.53	0.24	0.35	0.00	0.83	0.76	0.00	0.16	0.59	0.00	0.20
220	222.39	0.41	0.18	333.33	0.58	0.17	0.33	0.00	0.82	0.76	0.00	0.13	0.59	0.00	0.17

Table 29. Size and morphological parameters acquired with Microscope 2

Nominal Particle Size (µm), ABD	**ABD (µm)**	SD (µm)	RSD (%)	**MFD (µm)**	SD (µm)	RSD (%)	**Circularity**	SD	RSD (%)	**AR**	SD	RSD (%)	**Round**	SD	RSD (%)
100	99.91	0.41	0.41	148.80	0.42	0.28	0.35	0.00	1.07	0.76	0.00	0.40	0.59	0.00	0.25
150	149.04	0.57	0.38	222.47	0.74	0.33	0.34	0.00	1.19	0.76	0.00	0.24	0.59	0.00	0.27
220	222.27	0.34	0.15	333.58	0.30	0.09	0.33	0.00	0.83	0.76	0.00	0.11	0.59	0.00	0.14

12. References

1. Sauna ZE, Richards SM, Maillere B, Jury EC, Rosenberg AS. Editorial: Immunogenicity of Proteins Used as Therapeutics. Front Immunol. 2020;11:614856. doi: 10.3389/fimmu.2020.614856.
2. Ratanji KD, Dearman RJ, Kimber I, Thorpe R, Wadhwa M, Derrick JP. Editor's Highlight: Subvisible Aggregates of Immunogenic Proteins Promote a Th1-Type Response. Toxicol Sci. 2016;153(2):258-70. doi: 10.1093/toxsci/kfw121.
3. Ratanji KD, Derrick JP, Dearman RJ, Kimber I. Immunogenicity of therapeutic proteins: influence of aggregation. J Immunotoxicol. 2014;11(2):99-109. doi: 10.3109/1547691X.2013.821564.
4. Ayres JD. Conducting Clinical Risk Assessments for Visible Particulate Matter in Parenteral Preparations. PDA J Pharm Sci Technol. 2018;72(6):626-39. doi: 10.5731/pdajpst.2018.008615.
5. Doessegger L, Mahler HC, Szczesny P, Rockstroh H, Kallmeyer G, Langenkamp A, et al. The potential clinical relevance of visible particles in parenteral drugs. J Pharm Sci. 2012;101(8):2635-44. doi: 10.1002/jps.23217.
6. USP <790> Visible Particulates in Injections. The United States Pharmacopeia Convention National Formulary. 2016;USP 39 NF 32. doi: 10.31003/USPNF_M7197_01_01.
7. USP <1790> Visual Inspection of Injections. The United States Pharmacopeia Convention National Formulary. 2017;USP 40 NF 35. doi: 10.31003/USPNF_M7198_06_01.
8. Telikepalli SN, Carrier MJ, Ripple DC, Barnett G, Bhirde A, Bolton D, et al. An Interlaboratory Study to Identify Potential Visible Protein-Like Particle Standards. AAPS PharmSciTech. 2022;24(1):18. doi: 10.1208/s12249-022-02457-9.
9. Schindelin J, Arganda-Carreras I, Frise E, Kaynig V, Longair M, Pietzsch T, et al. Fiji: an open-source platform for biological-image analysis. Nat Methods. 2012;9(7):676-82. doi: 10.1038/nmeth.2019.
10. International Organization of Standardization (2014). Particle Size Analysis-Image Analysis Methods-Part 1: Static Image Analysis Methods (ISO Standard No. 13322-1). http://www.iso.org/standard/51257.html.
11. Skene DS. The effect of refractive index of the mounting medium on the apparent diameter of latex particles and glass fibres. Journal of Microscopy. 1969;89(1):63-71. doi: 10.1111/j.1365-2818.1969.tb00650.x.
12. Bates D. MM, Bolker B., Walker S. . Fitting Linear Mixed-Effects Models Using lme4. Journal of Statistical Software. 2015;67(1):1-48. doi: 10.18637/jss.v067.i01.
13. Team RC. R: A language and environment for statistical computing. R Foundation for Statistical Computing. Vienna, Austria2021; Available from: https://www.R-project.org/.
14. DerSimonian R. LN. Meta-analysis in clinical trials Control. Controlled Clinical Trials. 1986;7:177-88. doi: 10.1016/0197-2456(86)90046-2.
15. Viechtbauer W. Conducting meta-analyses in R with the metafor package. Journal of Statistical Software. 2010;36(3):1-48. doi: 10.18637/jss.v036.i03.
16. Ferreira TR, W. ImageJ/Fiji 1.46 User Guide. 2012. http://imagej.net/ij/docs/guide/146.html.

17. Ripple D, Srivalli Telikepalli, Kristen Steffens, Michael Carrier, Christopher Montgomery, Nicholas Ritchie, Z.Q. John Lu. (2019), Reference Material 8634 Ethylene Tetrafluoroethylene for Particle Size Distribution and Morphology, Special Publication (NIST SP), National Institute of Standards and Technology. doi:10.6028/NIST.SP.260-193.
18. Schroeder S, Braun S, Mueller U, Sonntag R, Jaeger S, Kretzer JP. Particle analysis of shape factors according to American Society for Testing and Materials. J Biomed Mater Res B Appl Biomater. 2020;108(1):225-33. doi: 10.1002/jbm.b.34382.